Materials for Electronics

The U.S. electronics industry faces strong international competition in the manufacture of smaller, faster, more functional, and more reliable products. Many critical challenges facing the industry require the continual development of advanced materials and processes. The NIST Materials Science and Engineering Laboratory (MSEL) works closely with U.S. industry covering a broad spectrum of sectors including semiconductor manufacturing, device components, packaging, data storage, and assembly, as well as complementary and emerging areas such as optoelectronics and organic electronics. MSEL has a multidivisional approach, committed to addressing the most critical materials measurement and standards issues for electronic materials. Our vision is to be the key resource within the Federal Government for materials metrology development and will be realized through the following objectives:

- Develop and deliver standard measurements and data;
- Develop advanced measurement methods needed by industry to address new problems that arise with the development of new materials;
- Develop and apply *in situ* as well as real-time, factory floor measurements, for materials and devices having micrometer- to nanometer-scale dimensions;
- Develop combinatorial material methodologies for the rapid optimization of industrially important electronic materials;
- Provide the fundamental understanding of the divergence of thin film and nanoscale material properties from their bulk values;
- Provide the fundamental understanding of materials needed for future nanoelectronic devices, including first principles modeling of such materials.

The NIST/MSEL program consists of projects led by the Metallurgy, Polymers, Materials Reliability, and Ceramics Divisions. These projects are conducted in collaboration with partners from industrial consortia (*e.g.*, International SEMATECH), individual companies, academia, and other government agencies. The program is strongly coupled with other microelectronics programs within the government such as the National Semiconductor Metrology Program (NSMP). Materials metrology needs are also identified through the International Technology Roadmap for Semiconductors (ITRS), the IPC Lead-free Solder Roadmap, the National Electronics Manufacturing Initiative (NEMI) Roadmap, the Optoelectronics Industry Development Association (OIDA) Roadmap, IPC (the International Packaging Consortium), and the National [Magnetic Data] Storage Industry Consortium (NSIC) Roadmap.

In each of these areas, MSEL researchers have made substantial contributions to the most pressing technical challenges facing industry, from new fabrication methods and advanced materials in the semiconductor industry, to advanced packaging materials, to magnetic data storage. Below are just a few examples of MSEL contributions over the past year.

Advanced Gate Dielectrics

To enable further device scaling, the capacitive equivalent thickness (CET) of the gate stack thickness must be 0.5 nm to 1.0 nm. This is not achievable with existing SiO_2/polcrystalline Si gate stacks. Given the large number of possible choices for these new layers, the only feasible approach to understanding the complex materials interactions that result at the gate dielectric/substrate and gate dielectric/metal gate electrode interfaces is through the application of combinatorial methodologies. This same methodology and apparatus are applicable to a wide variety of problems in the electronic materials field.

Sub-100 nm Nanofabrication

The continual decrease in feature size has been the driving force for advances in the semiconductor industry. Current structures have 90 nm dimensions with planned nodes at 65 nm and 35 nm structures. Advanced measurements of the patterning materials (photoresists), are needed to enable future large scale manufacturing of smaller devices. MSEL utilizes advanced x-ray and neutron tools to provide insight into the feasibility and optimization of these important processes.

Advanced Metallization

Electrodeposited copper is rapidly replacing aluminum for on-chip “wiring” because of its lower electrical resistivity, superior electromigration behavior, and the ability to fill fine features without the formation of seams or voids. As feature dimensions go below 100 nm, difficulties in maintaining performance are anticipated. These issues are addressed through a combination of modeling and experimental efforts.

Test Methods for Embedded Passive Devices

Significant advantages arise if passive devices are integrated directly into the circuit board as embedded passive devices rather than discretely attached with automated assembly. New metrology methods were developed to address the needs of the electronic industry. Two test methods were completed and have received wide acceptance by industry as new methods to accelerate the development of embedded passive device technology.

Table of Contents

Materials for Electronics

Ceramics

Combinatorial Tools for Materials Science 1

Spectroscopy, Diffraction, and Imaging of Electronic Materials 2

Phase Equilibria and Properties of Dielectric Ceramics 3

Phase Relations of High T_c Superconductors 4

Metrology and Standards for Optoelectronic Materials 5

Experimental and Theoretical Influence of Thin Film Texture on Ferroelectric Hysteresis 6

Theory and Modeling of Dielectric Materials 7

Materials Reliability

Electronic Packaging and Components

Electronic Packaging and Components: Packaging Reliability 8

Electronic Packaging and Components: Acoustic Characterization 9

Micrometer-Scale Reliability

Micrometer-Scale Reliability: Mechanical Behavior of Thin Films 10

Micrometer-Scale Reliability: Chip-Level Interconnects 11

Micrometer-Scale Reliability: Dynamic Imaging of Magnetic Domain Walls 12

Micrometer-Scale Reliability: Bridging Length Scales 13

Micrometer-Scale Reliability: Molecular Dynamics 14

Micrometer-Scale Reliability: Solder Reliability 15

Metallurgy

Combinatorial/Phase Diagram Approach for Metallization to Wide-Band-Gap Semiconductors 16

Lead-Free Surface Finishes: Sn Whisker Growth 17

Lead-Free Solders and Solderability 18

Electrical Properties of On-Chip Interconnections 19
Nanomagnetodynamics 20
Electrodeposited $Pt_{1-x}(Fe,Co,Ni)_x$Alloys 21
Novel Magnetic Materials for Sensors and
Ultra-High Density Data Storage 22
Discovery of Spin Density Waves in a Ferromagnet: Fe-Al 23

Polymers

Characterization of Porous Low-k Dielectric Constant Thin Films 24
Polymer Photoresists for Next-Generation Nanolithography 25
Organic Electronics 26
Nanoimprint Lithography 27

Combinatorial Tools for Materials Science

Combinatorial materials science has rapidly become a new paradigm for the acceleration of materials research. It is a fast and efficient methodology for materials optimization and discovery, characterized by high throughput, parallel experiments, automated analysis, and massive data sets. NIST's industrial stakeholders are identifying it as the only viable technique for understanding complex materials science systems in a competitive timeframe. Its application to a critical materials science problem in the Si microelectronics industry, the replacement of the gate stack, is expected to drive an inorganic combinatorial materials science program at NIST.

Martin L. Green

NIST/MSEL is poised to play several important roles in developing combinatorial materials methodologies, especially as they pertain to industrially important, advanced inorganic materials. Included in this class are materials such as thermoelectrics, dielectric and metal layers for advanced Si CMOS gate stacks, multiferroics, magnetic semiconductors for spintronics, transparent semiconductors, and fuel cell and H_2 storage materials. NIST/MSEL has an opportunity to take a lead position in the use of combinatorial methodologies for:

- New, combinatorially-friendly (rapid, local, microscopic measurements) metrologies;
- Materials optimization and development;
- Means of experimentally verifying computed materials properties;
- Tools for determining phase diagrams and other property data; and
- "Data on demand," or "just-in-time-data."

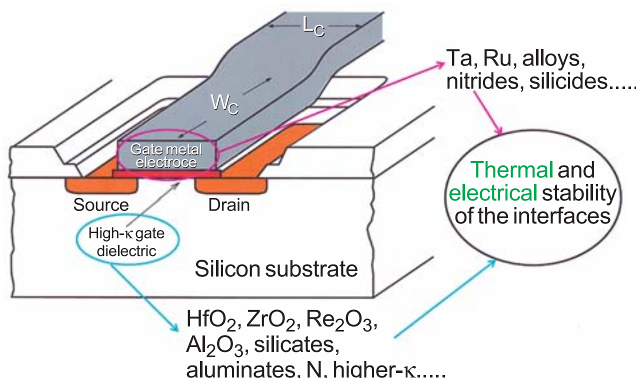

Figure 1: *MOSFET device with advanced gate stack.*

The advanced gate stack application for Si CMOS is a good example. International Sematech (ISMT) is currently faced with major materials challenges to further miniaturization. Figure 1 schematically illustrates a metal oxide-semiconductor field effect transistor (MOSFET), showing the advanced gate stack which consists of the high-κ (κ = dielectric constant) gate dielectric and the metal gate electrode. To enable further device scaling, the capacitive equivalent thickness (CET) of the gate stack thickness must be 0.5 nm to 1.0 nm. This will not be achievable with existing SiO_2/polycrystalline Si gate stacks. Given the large number of possible choices for these new layers, the only feasible approach to understanding the complex materials interactions that result at the gate dielectric/substrate and gate dielectric/metal gate electrode interfaces is through the application of combinatorial methodologies.

The acquisition of a state-of-the-art combinatorial synthesis tool is expected be one of the cornerstones of the NIST/MSEL effort. In addition, we plan to acquire combinatorially-friendly tools such as a micro-x-ray diffractometer, and to develop new metrologies such as nanocalorimetry for the detection of phase transformations in thin films.

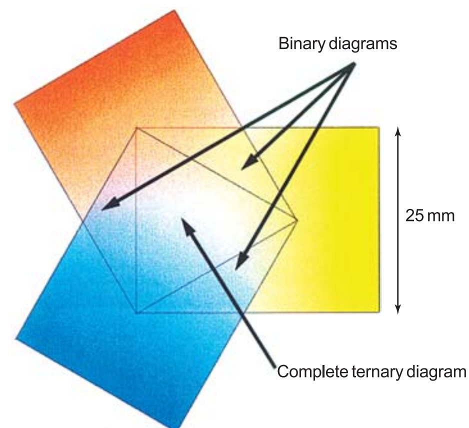

Figure 2: *Combinatorial ternary and binary film libraries.*

The new combinatorial synthesis tool will be capable of depositing entire ternary and binary libraries in areas as small as 6.5 cm^2 (1 in^2), as is shown in Figure 2.

Contributors and Collaborators

L. Cook, W. Wong-Ng, P. Schenck (Ceramics Division, NIST); L. Bendersky, A. Davydov (Metallurgy Division, NIST); S. Semancik (CSTL, NIST); J. Suehle, E. Vogel (EEEL, NIST); T. Chikyow (NIMS, Japan); B. Murto (International Sematech); I. Takeuchi (U. of Maryland)

Spectroscopy, Diffraction, and Imaging of Electronic Materials

Modern electronic devices have reached the point where fundamental materials properties now limit continued improvement in device performance. Consequently, new materials, their synthesis, their properties, and their interactions with established materials and technologies are in continuous need of development and investigation. The Ceramics Division operates a suite of synchrotron beamlines, at the Advanced Photon Source and at the National Synchrotron Light Source, designed to address critical issues focused on these next-generation materials, including the electronic and structural properties of materials used in advanced electronic applications.

Joseph C. Woicik

The electronics industry is seeking to increase device performance by increasing carrier mobility in silicon by introducing a small tensile strain into the silicon lattice. This is accomplished by the epitaxial growth of a thin silicon layer on a virtual crystalline substrate of relaxed $Si_{1-x}Ge_x$ with x typically between 10 % and 50 %. A critical aspect of this process is the control of defects in the SiGe-alloy layer and the propagation of these defects into the strained-Si film.

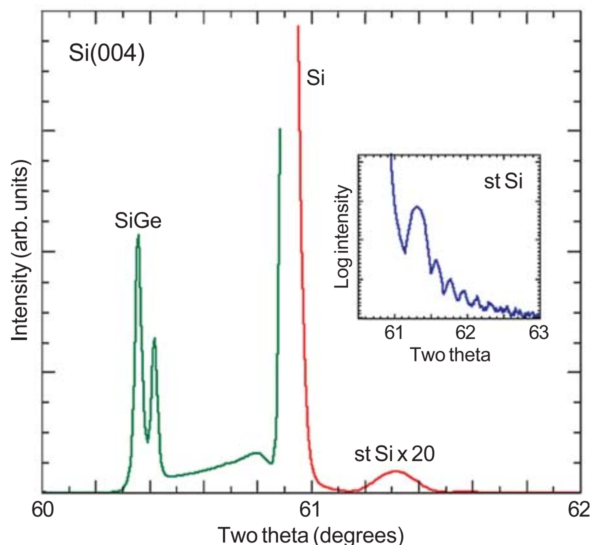

Figure 1: *Radial diffraction scan for a strained-Si/Si_xGe_{1-x}/Si(001) semiconductor layered structure.*

We have utilized x-ray diffraction and x-ray topography at the UNICAT beamline facility at the Advanced Photon Source to image defects in the SiGe film and to study how these defects propagate into the strained-Si overlayer. Figure 1 shows a high-resolution x-ray diffraction scan around the Si(004) Bragg condition from a 500 Å Si film grown on a relaxed 3 µm thick SiGe film with a Ge content of 20 %. The relaxed SiGe film was grown on top of a SiGe layer that was grown on a Si(001) substrate and graded in composition from 0 % to 20 % Ge content over a thickness of 2 µm.

The diffraction from the SiGe is seen near $2\theta = 60.4°$; it appears as a doublet due to a slight composition variation due to the intermediate planarization process. Diffraction from the grade is also apparent. The sharp peak near $2\theta = 60.9°$ is diffraction from the Si substrate, and the much weaker peak near $2\theta = 61.3°$ is diffraction from the strained-Si film. The Si film has a smaller perpendicular lattice constant than the crystalline Si substrate because it is under in-plane tensile strain due to its epitaxy with the SiGe layer that possesses a larger cubic lattice constant.

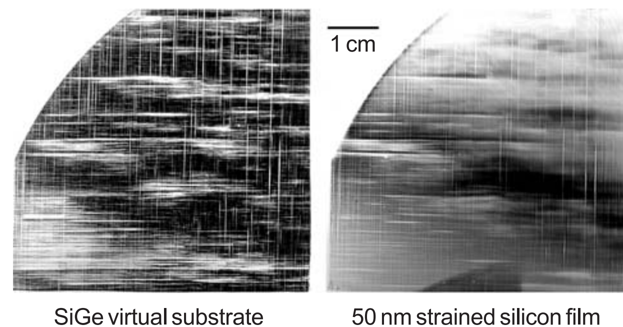

Figure 2: *(113) x-ray topographs of the SiGe film and the strained-Si overlayer.*

The differences in lattice constants between the strained-Si film, SiGe layer, and Si substrate make it possible to image the diffraction from each component separately. Figure 2 shows the (113) x-ray topographs recorded with an x-ray energy of ≈ 8.9 keV. This diffraction geometry was chosen because it is within Si total external reflection and, therefore, limits the x-ray penetration depth into the sample.

The microstructure of the substrate and film are nearly identical, demonstrating that the misfit-dislocation structure responsible for the relaxation of the SiGe layer acts as a template for the microstructure of the strained-Si film. The crystallographic nature of these defects and their contribution to the ultimate relaxation of the strained-Si film are currently under investigation.

Contributors and Collaborators

D. Black, I. Levin (Ceramics Division, NIST); M. Erdtmann, T.A. Langdo (AmberWave)

Phase Equilibria and Properties of Dielectric Ceramics

Ceramic compounds with exploitable dielectric properties are widely used in technical applications such as actuators, transducers, capacitors, and resonators or filters for microwave communications. Phase equilibria determination integrated with systematic chemistry–structure-property studies contribute toward the fundamental understanding and rational design of these technologically important materials with improved properties and/or reduced processing costs.

Terrell A. Vanderah, Igor Levin, and Michael W. Lufaso

Cost and performance are the primary and secondary drivers, respectively, for today's commercial needs in the area of dielectric ceramics. For example, component suppliers and builders of 2 GHz cellular infrastructure are critically impacted by the high cost of tantalum-containing ceramics needed for dielectric resonators: only a single ceramic material, perovskite-like $Ba_3ZnTa_2O_9$ (BZT), is available with the needed properties. Interest is keen to reduce its processing costs or to find an alternative, less-expensive substitute. The results of an experimental phase equilibria study of the system (Figure 1) revealed that BZT ceramics must be processed so that ZnO volatilization occurs along the two-phase join between BZT and $Ba_8ZnTa_6O_{24}$ (8L) to prevent the formation of deleterious air-sensitive compounds high in BaO content, or dielectrically poor "TTB" type phases.

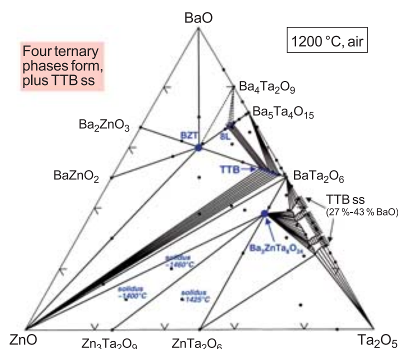

Figure 1: Phase equilibria diagram determined for the system containing the important commercial ceramic $Ba_3ZnTa_2O_9$ (BZT).

A potential replacement for BZT is the analogous compound with less costly niobium, $Ba_3ZnNb_2O_9$. The phase equilibrium diagram determined for this system (Figure 2) provides processing information for this ceramic and clearly indicates that its dielectric loss cannot be improved by liquid-phase sintering in the presence of low-melting, electrically acceptable $ZnNb_2O_6$, because the two compounds do not occur in equilibrium with each other. Such mixtures, instead, will form dielectrically poor impurity phases.

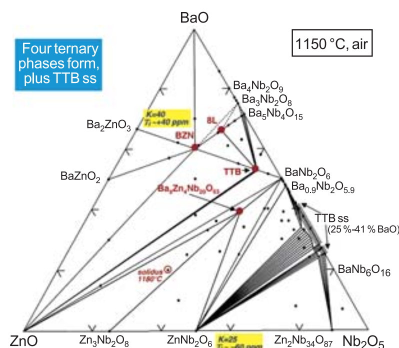

Figure 2: Phase equilibria diagram determined for the system containing $Ba_3ZnNb_2O_9$ (BZN), a possible BZT alternative.

Systematic studies of the $Ba_3MNb_{2-x}Sb_xO_9$ (M = Mg, Ni, Zn), system were carried out to manipulate the crystal chemistry and high-frequency (> 2 GHz) dielectric properties by progressive substitution of Sb^{5+} (d^{10}) for Nb^{5+} (d^0). The results showed that control of permittivity and tuning of the temperature coefficient to zero was possible with appropriate substitution. Optimal dielectric losses were obtained for specimens with low x-values and 2:1-type ordered perovskite structures.

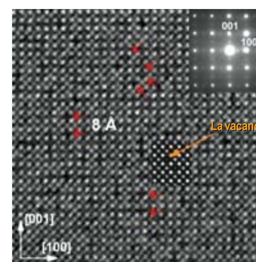

Figure 3: HRTEM image of 50:50 $LaMg_{1/2}Ti_{1/2}O_6$-$La_{2/3}TiO_3$. Dark crosses denote La vacancies, deduced from image simulations (insert). Short-range order of La vacancies is revealed as pairs of dark crosses in both the [001] and [100] directions and causes diffuse superlattice reflections in the diffraction pattern.

Detailed structural studies of the $LaMg_{1/2}Ti_{1/2}O_6$-$La_{2/3}TiO_3$ solid solution were carried out to elucidate the origin of the anomalous changes in permittivity and temperature coefficient near 50:50. The results showed that the abrupt changes in properties were accompanied by the disappearance of one octahedral tilting mode and the onset of short-range ordering of La vacancies.

Contributors and Collaborators

W. Wong-Ng, R.S. Roth, B. Burton, E. Cockayne (Ceramics Division, NIST); J.E. Maslar (Process Measurements Division, NIST); R. Geyer (Radio Frequency Technology Division, NIST); S. Bell (TCI Ceramics)

Phase Relations of High T_c Superconductors

Phase equilibria data are needed for quality control, cost reductions, performance enhancements, and optimal processing in high T_c technology. These needs are being addressed through studies of the phase equilibria and kinetics of $Ba_2YCu_3O_{6+x}$ formation from barium fluoride amorphous precursor films, determination of $Ba_2RCu_3O_{6+x}$ (R=Dy,Yb) phase diagrams, and investigations of superconductor/buffer layer interactions: all play critical roles in the development of RABiTS/IBAD coated conductor technology.

Winnie Wong-Ng, Lawrence P. Cook, and Igor Levin

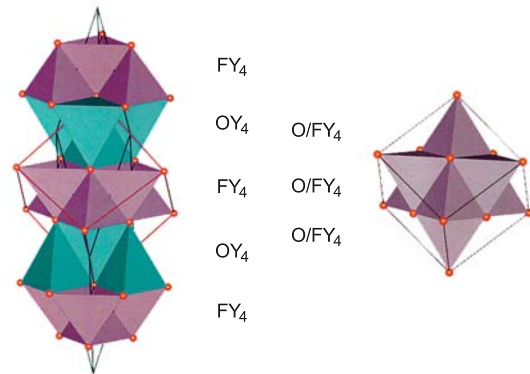

Figure 1: *Schematic of the YOF rhombohedral structure (left, showing layers of $[OY_4]$ and $[FY_4]$ tetrahedra) and the cubic fluorite structure (right).*

Phase diagrams serve as "blue prints" for successful processing of high T_c superconductor materials. In the past year, as an integral part of the DOE intensive R&D program on high T_c wire and cable applications, we have continued to provide critical data for the development of practical superconductors. Our research was related to two groups of superconductors: (1) $Ba_2RCu_3O_7$ (R=Dy, Yb) coated conductors produced by rolling assisted biaxially textured substrate/ion beam assisted deposition (RABiTS/IBAD); and (2) MgB_2.

Our main effort has been focused on the determination of $BaO\text{-}R_2O_3\text{-}CuO_x$ phase relations as a function of oxygen pressure, p_{O2}, and choice of lanthanides. These studies were completed under carbonate-free conditions, to match better the processing conditions of RABiTS/IBAD conductors. This year we have completed the study of the two systems with R= Dy and Yb. A trend in phase formation and tie-line $Ba_2RCu_3O_7$ relationships was observed in the present work which provides a general correlation for R=Nd, Sm, Eu, Gd, Dy, Ho, Y, Er, and Yb with respect to the size of the lanthanides. In collaboration with Brookhaven National Laboratory and California Institute of Technology, an understanding of the effect of strain on the trend of the orthorhombic to tetragonal phase transition temperature of $Ba_2RCu_3O_7$ was obtained through modeling. By mixing the smaller lanthanides R′ with the larger R in the $Ba_{2-x}(R_{1+x-y}R'_y)Cu_3O_{6+z}$ superconductor, both flux-pinning and melting properties can be tailored and optimized. A trend in solid solution extent as related to the size of R was observed in $Ba_{2-x}(R_{1+x-y}Y_y)Cu_3O_z$ (R= Sm, Eu and Gd).

The "BaF_2 *ex-situ*" process is a promising method for production of $Ba_2YCu_3O_7$ superconducting wire and cable. Previously, using a controlled-atmosphere apparatus, we determined the presence of low-temperature liquids in the multicomponent reciprocal Ba-Y-Cu//O,F system. This year, we identified YOF (Figure 1) as an important intermediate phase in the system with a low temperature reversible order–disorder phase transition near the initial melting of fluoride-rich melts. These more detailed studies have allowed better definition of the region of low-temperature melting. Also, phase diagrams of the pertinent subsystems of $BaO\text{-}Y_2O_3\text{-}CeO_2\text{-}CuO_x$ representing the interaction of product $Ba_2YCu_3O_7$ with the CeO_2 buffer layer were determined.

To control film properties, it is important to understand the details of $Ba_2YCu_3O_7$ formation from "BaF_2" films. High temperature x-ray diffraction and transmission electron microscopy have been applied to compare the detailed conversion mechanism of films prepared with different precursors on $SrTiO_3$ substrates and on RABiTS substrates (both provided by ORNL). A phase with a $Ba(O_xF_y)$-based superlattice has been found to be involved as an intermediate product. Its presence may prove to be an important factor influencing the kinetics of $Ba_2YCu_3O_7$ formation.

Studies on MgB_2 also continued with measurements of the enthalpy of formation (by solution calorimetry) and vapor pressure (by thermogravimetric effusion). Attention was focused on the significant sources of variability in these properties. These data are essential for reproducible processing of MgB_2 films, wire and cable.

Contributors and Collaborators

Q. Huang (NIST Center for Neutron Research); M. Vaudin, P. Schenck (Ceramics Division, NIST); R. Shull (Metallurgy Division, NIST); R. Klein (Biotechnology Division, NIST); R. Feenstra, A. Goyal (ORNL); T. Holesinger (LANL); M. Rupich (ASC); J. Kaduk (BP-Amoco); T. Haugan (U.S. Air Force); P. Canfield (Ames Lab); R. Meng (U. of Houston); D. Welch (BNL), H.B. Su (Caltech)

Metrology and Standards for Optoelectronic Materials

The optoelectronics industry needs measurement techniques and accurate materials property data to calibrate their deposition processes and to evaluate both prototype and finished devices. Recent work has focused on the electronic band structure of InGaAsN films (for infrared detectors and solar cells) and calibration of strain in ultrathin $Al_xGa_{1-x}As$ films and optical properties of GaN and ZnO nanowire structures.

Albert J. Paul and Lawrence H. Robins

$In_yGa_{1-y}As_{1-x}N_x$ semiconductor alloy films show promise for infrared optoelectronic devices. Data on the electronic band structure are needed to facilitate device design and simulation. We examined Si-doped $In_yGa_{1-y}As_{1-x}N_x$ films with $x < 0.012$ and $0.052 < y < 0.075$ by photoreflectance (PR) spectroscopy, supplemented by secondary ion mass spectroscopy (SIMS) and energy dispersive x-ray spectroscopy (EDS, for composition), XRD (strain), and Hall effect (electrical properties). The composition and carrier concentration dependence of the critical point energies, designated E_- (fundamental gap), $E_-+\Delta_{SO}$ (split-off valence band to conduction band), and E_+ (valence band to nitrogen impurity band) was successfully explained by a band anti-crossing and free-carrier band-filling model with a small number of adjustable parameters.

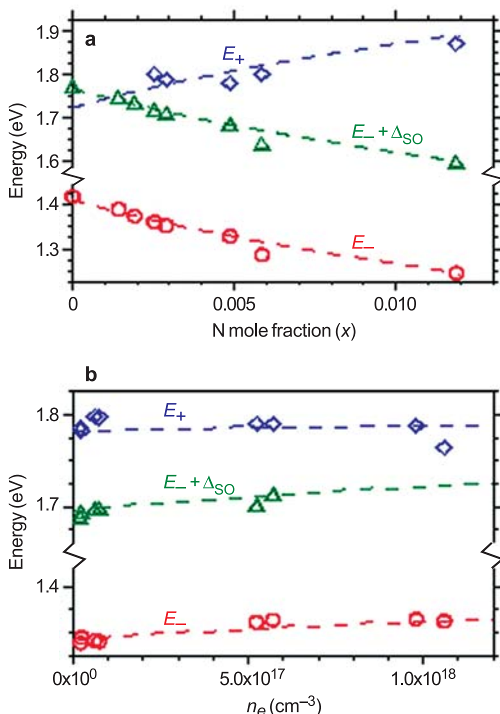

Figure 1: *PR critical-point energies: data and modeling.*

The measured critical-point energies (symbols) and the best-fit model (dashed curves) are plotted as functions of N mole fraction (x) in Figure 1(a), and Hall carrier concentration (n_e) in Figure 1(b).

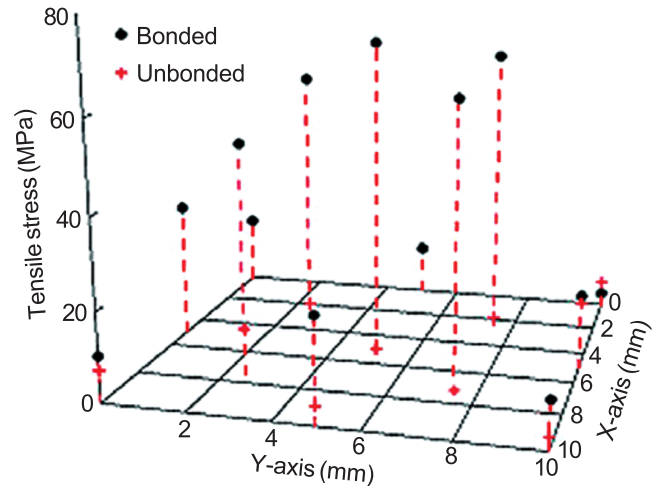

Figure 2: *Tensile stress distributions in two $Al_{0.2}Ga_{0.8}As$ structures, obtained from calibrated PL measurements.*

We are continuing to develop methods for quantifying optical measurements of stress and strain in III–V semiconductors. By calibrating the shift of the Raman and PL peaks with known applied stress in a load cell, we are able to measure stresses due to differential thermal expansion, film-substrate lattice mismatch, and device packaging. As an example, the stress induced by bonding of a 10 mm × 10 mm $Al_{0.2}Ga_{0.8}As$-on-GaAs sample (grown as a composition SRM) to a stainless steel disk was measured by this technique. Results from selected locations on the bonded sample and, for comparison, an unbonded piece cut from the same wafer, are shown in Figure 2. A large tensile stress is seen to occur near the center of the bonded piece, but not in the unbonded piece.

Stress measurements of ultrathin (5 nm to 30 nm) AlGaAs films have been initiated to compare spatially resolved measurements of stress near the edges of ultrathin films with the quantitative predictions of Object-Oriented Finite Element (OOF) modeling.

Contributors and Collaborators

E. Fuller, Y.-S. Kang, G. White (Ceramics Division, NIST); K.A. Bertness, N.A. Sanford (Optoelectronics Division, NIST); A.V. Davydov, A.J. Shapiro (Metallurgy Division, NIST); D. Chandler–Horowitz (Semiconductor Electronics, NIST); M.M.E. Fahmi, S.N. Mohammad (Howard University)

Experimental and Theoretical Influence of Thin Film Texture on Ferroelectric Hysteresis

Commercial ferroelectric thin film devices are rapidly approaching the same nanoscale dimensions as individual grains, yet little is known about the influence of grain boundaries and local texture on ferroelectric properties. Accordingly, several complementary experimental and theoretical techniques are being developed to assess the local ferroelectric response. By combining quantitative piezoelectric force microscopy (PFM), electron backscattering diffraction (EBSD), and two-dimensional object oriented finite-element modeling (OOF), various individual crystallographic distributions with either beneficial or detrimental effects can be identified and eventually predicted.

Bryan D. Huey, R. Edwin García and John E. Blendell

Crystallographic orientation can now be determined with nanometer scale lateral resolution using the newly installed electron backscattering diffraction system (EBSD), allowing the orientation of individual ferroelectric grains to be mapped as indicated in Figure 1a.

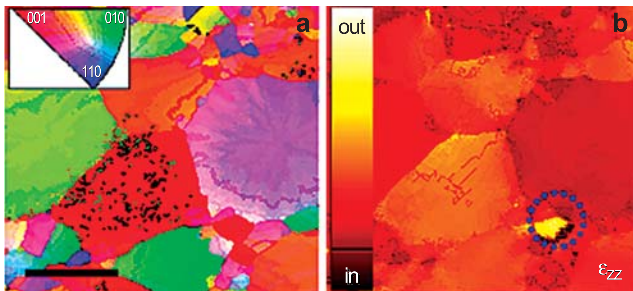

Figure 1: (a) Measured surface orientation of PZT thin film and (b) predicted strain normal to the surface for the same grains when biased with an electrode as indicated. Bar = 20 µm.

Recent advances in two-dimensional (2-d) object oriented finite element modeling (OOF) have made it possible to predict the piezoelectric response of a polycrystalline thin film with full consideration of the sample texture as determined by EBSD. Figure 1b demonstrates the strain normal to the surface for an applied bias of 1 V across a 100 nm thick film using a 100 nm diameter electrode, where the electrode is positioned across multiple grains of differing orientations. The local response is strongly dependent on texture, in some cases oppositely oriented.

Piezoelectric force microscopy (PFM) was employed to determine experimentally the ferroelectric

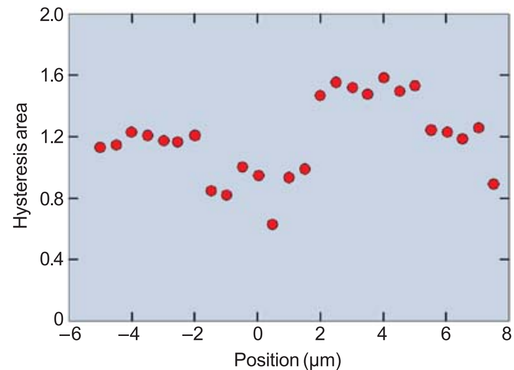

Figure 2: Measured piezoelectric hysteresis areas of several grains/boundaries.

properties of the same grain and grain boundary regions considered by EBSD and OOF. This AFM-based technique is widely used, but can be significantly hindered by several instrumental artifacts that were identified and overcome during this work. The area of piezoelectric hysteresis loops determined using the newly developed quantitative methods is indicated in Figure 2 for several distinct grains and boundaries. The measured hysteresis variations correlate with grains and grain boundaries of differing misorientation as measured by EBSD and correlates with strains calculated by OOF.

Key accomplishments and conclusions include:

1) Novel methods for identifying and overcoming artifacts in piezoelectric force microscopy to allow quantitative local piezoelectric hysteresis measurements;
2) Unique 2-d simulations of converse-piezo actuation with complete incorporation of true thin-film texture;
3) The importance of uniform texture for optimal ferroelectric properties when device dimensions approach the lateral grain size; and
4) The likelihood of domain pinning or even crack initiation at certain grain boundaries and intersections as a result of local orientation.

Results from this work were presented at the SPIE Ferroelectrics conference, American Ceramic Society annual meeting, European Congress on Nanoscale Materials (Nano-04), IEEE Ferroelectrics and Ultrasonics joint meeting, and several invited seminars at NIST and various universities. Publications in the *Journal of the American Ceramic Society*, *Journal of Electroceramics*, and *Journal of Applied Physics* are under review.

Contributors and Collaborators

M.D. Vaudin, E.R. Fuller, Jr. (Ceramics Division, NIST); S. Hong (Samsung)

Theory and Modeling of Dielectric Materials

Dielectric ceramics are widely used in applications such as semiconductor gate dielectrics, actuators, capacitors, and resonators or filters for microwave communications. For simple systems, first-principles (FP) methods allow direct calculations of low-temperature dielectric constants. For complex systems, and for rational new materials design, larger scale modeling is required. Multiscale effective Hamiltonian (EH) models derived from FP calculations retain high accuracy and allow phenomena caused by chemical ordering, defects, and changes in temperature to be explored. The EH provides a bridge from FP calculations (≤ 100 atoms) to the needed computations with hundreds of thousands of atoms. We are developing a methodology to enable automatic EH generation for real three-dimensional systems.

Eric Cockayne and Benjamin P. Burton

Materials that are optimized for industrial applications are generally solid solutions in which the configuration of ions on mixed ion sites strongly affects the physical properties. To model these phenomena, detailed FP calculations are performed on a variety of perfectly ordered systems. For example, $PbMg_{1/3}Nb_{2/3}O_3$ (PMN) is the main component of recently discovered materials with ultrahigh piezoelectric constants. PMN presents a singular challenge, because the details of Mg-Nb ordering are not fully known. To better understand PMN, we studied various PMN composition supercells with 15 to 30 atoms. A comparison of fully relaxed structures predicts a ground state ordering different from that previously assumed. The two lowest-energy structures found are most compatible with the "random site model" of PMN deduced from experiment. Calculated infrared spectra (directly related to the dielectric function) also show that the two lowest energy structures are most similar to experiment.

For the $(CaAl_{1/2}Nb_{1/2}O_3)_{1-x}$–$(CaTiO_3)_x$ (CAN-CT) system of microwave dielectric interest, a cluster expansion EH model for the low temperature dielectric constant was developed to calculate the dielectric constant for an arbitrary CAN-CT configuration as a function of x and Ti-Al-Nb ordering. Work is in progress to parameterize similar models for other solid solution systems.

Temperature dependent dielectric properties can be modeled with Monte Carlo and molecular dynamics simulations based on EHs. The EH for a heterovalent solid solution includes the random local electric fields generated by mixing differently charged ions in an alloy. We compiled a catalog of the possible local field directions in the nearest-neighbor approximation. By including local fields in an EH for $PbSc_{1/2}Nb_{1/2}O_3$ (PSN), we can reproduce the experimental observation that the dielectric peak of PSN, as a function of temperature, is broadened when nanoscale ordered domains are present.

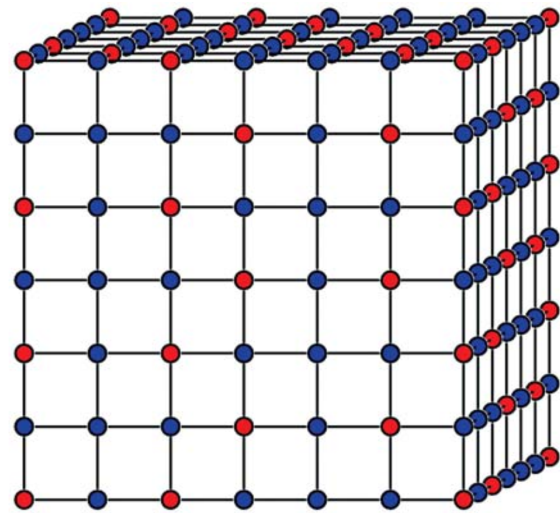

Figure 1: *Predicted ground-state ordering of Mg (red) and Nb (blue) in $PbMg_{1/3}Nb_{2/3}O_3$.*

Defects also affect physical properties. We computed the dipole moment of a Pb-O divacancy in $PbTiO_3$ from FP. Its moment is 2.28 e times the distance between the original Pb and O sites. The large electric fields produced by such defects have been incorporated into our EH for PSN.

Effective Hamiltonians for dielectrics and ferroelectrics are based on an efficient "lattice Wannier function" (LWF) description of the lattice dynamics of these systems. We have found a principle for automatically generating LWF and have demonstrated that it works on one-dimensional model systems. The method works equally well for chemically ordered systems, disordered systems, and systems with defects. This is a highly promising step towards automatic generation of effective Hamiltonians for real three-dimensional systems, which will make these EH methods accessible to non-experts.

Contributors and Collaborators

I. Levin, M. Lufaso, S. Tinte (Ceramics Division, NIST); P. Gehrig (NIST Center for Neutron Research, NIST); A. van de Walle (Northwestern U.); S.A. Prosandeev (Rostov State U.); U.V. Waghmare (JNCASR)

Electronic Packaging and Components: Packaging Reliability

We are developing methods to examine materials and interfaces in electronic packaging applications and elucidate the damage mechanisms. Our current focus is on advanced packaging structure, embedded passive materials, and thin metal films by use of thermal microscopy to measure heat flow and thermal properties on increasingly smaller size scales.

Andrew J. Slifka

Technical Description

The microelectronics industry is moving toward components of higher density and smaller size that use less expensive materials. One result of this is that reliability becomes an increasing concern due to coefficient of thermal expansion (CTE) mismatch and increased heat flow. As size decreases and functionality increases, thermomechanical fatigue becomes a factor in more areas of the microelectronics industry, including lead-free solders and interconnects.

We are investigating the structural damage induced from CTE mismatches between the various component materials in electronic packages to determine initiation of damage and the ultimate failure mechanisms. Thermal microscopy is used to measure changes in interfacial thermal resistance in order to detect the onset and continuation of thermomechanical damage, leading to electrical failure at interfaces.

We are developing new measurement methods using scanned-probe microscopy (SPM) in order to characterize packages and measure thermal conductivity of thin films at increasingly smaller size scales.

Accomplishments

We have completed measurements on industrial embedded resistors (see Figure 1), making comparative measurements between the SPM thermal system and the IR microscope.

We have made measurements of films by use of thermal SPM in a mode that uses the probe tip simultaneously as a point-source heater and a resistive element in a Wheatstone bridge circuit. For example, we have made preliminary measurements using various thicknesses of gold films on different substrates, and have compared a new theory, developed by our collaborators, to our measurements. Figure 2 shows data from a suite of these measurements. We will add interfacial modifications to the samples and to the theory in order to make the measurement method applicable to films used in industry. In addition, we have been using this measurement method on diamond-like-carbon (DLC) films. These industrial films are made from a polymer precursor, which allows easy and inexpensive coating onto various substrates. The thermal conductivity of these films, and how they compare to conventionally processed DLC films, is being investigated.

Finally, we are also measuring thermal conductivity of lead-free solder balls and interfacial thermal resistance between alloys and intermetallics.

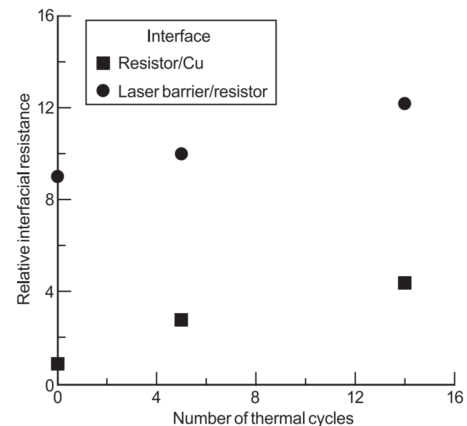

Figure 1: *Results of thermal SPM measurements on embedded resistor materials.*

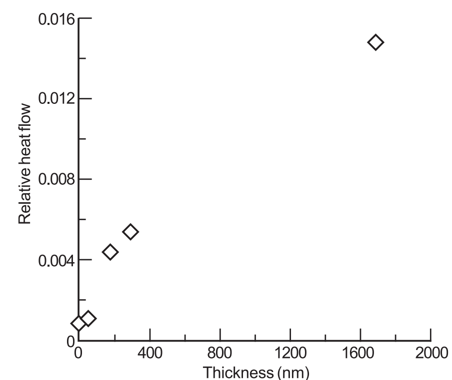

Figure 2: *Thermal SPM measurement results on various thicknesses of gold films on glass substrates.*

Contributors and Collaborators

J. Felten (DuPont Technologies, Research Triangle Park, NC); R. Snogren (SAS Circuits, Inc., Littleton, CO); K. Cole (University of Nebraska, Lincoln, NE); S. Joray (Cenymer Corp., Longmont, CO); F. Hua, (Intel Corp., Santa Clara, CA)

Electronic Packaging and Components: Acoustic Characterization

Bulk acoustic techniques have been developed and applied to the characterization of a variety of materials, with particular emphasis on piezoelectric crystals for electronic oscillator and filter applications. The research includes metrology of mode-selective noncontacting resonant spectroscopy, characterization of physical mechanisms that degrade performance of piezoelectric compounds with the structure of langasite, and determination of elastic constants of body-centered-cubic Ti and the shape-memory alloy NiTi.

Ward Johnson, Sudook Kim, and Carlos Martino

Over the past several decades, the Materials Reliability Division has established special capabilities in a variety of resonant acoustic techniques, including resonant ultrasound spectroscopy (RUS), time-domain resonance methods, noncontacting transduction, Marx-oscillator measurements, and torsional-pendulum measurements. The combined capability of these resonance systems enables elastic constants and anelastic damping to be measured from 4 K to 1100 K. The division also has implemented several conventional pulse-echo systems, including immersion scanning. During FY04, research was focused primarily on noncontacting mode selective metrology, analysis of anelastic damping in piezoelectrics, measurements of the temperature dependence of elastic constants of a shape-memory alloy, and determination of elastic constants of Ti in its high-temperature body-centered-cubic phase.

Langasite ($La_3Ga_5SiO_{14}$) and several of its isomorphs, including langatate ($La_3Ga_{5.5}Ta_{0.5}O_{14}$), have attracted significant attention in recent years as piezoelectric materials for improved electronic oscillators and filters. Research in our lab over the past year has sought to identify the dominant anelastic mechanisms that degrade the performance of these materials. An algorithm has been developed for fitting the measured temperature and frequency dependences of the mechanical Q to a superposition of loss mechanisms. For langasite, three point-defect relaxations are shown to be superimposed on a contribution that increased monotonically with temperature. In langatate, very similar anelastic effects appear, with distributions of activation energies that apparently arise from variations in residual stress.

To enable robust measurement of elastic constants of trigonal piezoelectric crystals, such as langasite,

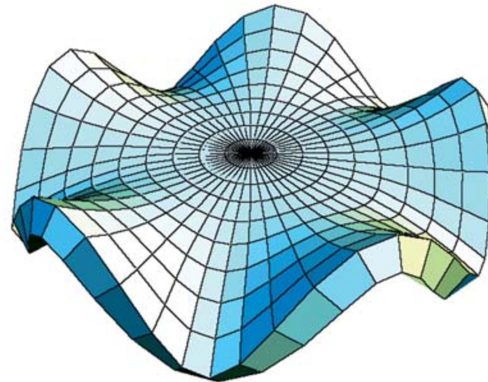

Figure 1: *Vibrational mode of a sapphire disk.*

methods of selectively measuring and analyzing resonant frequencies of modes with specified symmetry have been developed. This approach overcomes errors in analysis that can arise from misidentification of modes. The research has included measurements and analysis of quartz cylinders and sapphire disks. Noncontacting piezoelectric coupling with switchable electrode configurations and Ritz inversion algorithms including full symmetry information have been developed.

In collaboration with Los Alamos National Lab, analysis of resonance measurements on polycrystalline Ti at 1270 K were performed. Polycrystalline elastic constants were determined using the Ritz method. Then, the Kröner model was used to estimate monocrystalline constants from these polycrystalline constants.

Measurements of the temperature dependence of the elastic constants of the shape-memory alloy NiTi have been pursued in collaboration with the Mechanical Engineering Department of the University of Colorado. This study determined the effects of metallurgical treatments on the martensitic transition temperature and elastic constants. Pulse-echo measurements of elastic constants were performed on cold-drawn and hot-rolled specimens from 155 K to 300 K. Large Poisson ratios (> 0.4) reflect the material's superelasticity. Information was obtained on the hysteresis in elastic constants arising from the phase transition, which is a subject of controversy.

Contributors and Collaborators

P. Heyliger (Colorado State Univ.); M. Dunn, K. Gall (Univ. of Colorado, Mechanical Engineering Dept.); H. Ogi (Osaka Univ., Japan); H. Ledbetter (Los Alamos National Lab); A. Teklu (Univ. of Mississippi, Oxford)

Micrometer-Scale Reliability: Mechanical Behavior of Thin Films

Measurement methods and materials data are needed for the design of interconnect structures in high-performance integrated circuits. These micro- and nanometer-scale thin films are formed by physical vapor deposition; their microstructures, and hence their mechanical properties, are quite different from those of bulk materials of the same chemical composition. The ultimate goals of this project are to characterize the exact materials used in IC fabrication, at their proper size scale, and to understand the relevant deformation and failure mechanisms.

David T. Read

Interconnect structures in advanced integrated circuits carry power, signals, and heat from the transistors to the outside environment. These structures consist of multiple layers of thin films of conductors and dielectrics with barrier and adhesive layers. These thin films are an essential component of all advanced electronic devices, and similar materials are used in a variety of other applications, such as reflective coatings. Industry is aggressively pressing new materials into service, reducing the size of the structures, and requiring more functionality, including mechanical functionality, from all components of their structures. Design of reliable structures relies on quantitative numerical modeling, which requires accurate material property data. Because the films are formed by physical vapor deposition, their microstructures, and hence their mechanical properties, are quite different from those of bulk materials of the same chemical composition.

The objectives of this project are:

- To develop experimental techniques to measure the mechanical properties of thin films, in specimens fabricated and sized like materials used in actual commercial devices;
- To relate thin-film mechanical behavior to microstructure;
- To extend test techniques from their present level (1 μm thick, 10 μm wide) to smaller specimens that are similar in size to the conductive traces used in contemporary VLSI circuits (widths of 0.1 to 1 μm).

In previous years we reported properties of aluminum, polyimide, and polysilicon films at room temperature. We have now measured the tensile properties of aluminum films from a commercial source, and lab-made electrodeposited copper films from room temperatures up to 150 ºC. The mechanical properties decline only slightly with increasing temperature, in a pattern normal for face-centered-cubic metals.

Microtensile Young's (elastic) modulus data for nickel were contributed to a comparison study. The microtensile value was 177 ± 8 GPa (most probable uncertainty). Details are given elsewhere, but the conclusion from the full set of measurements is that both the modulus and the density of this sputtered nickel film are lower than bulk values. Microtensile modulus measurements, in particular, have been suspect because the results are often lower, by 10 % or more, than bulk values. See the Molecular Dynamics page of this report for more on this.

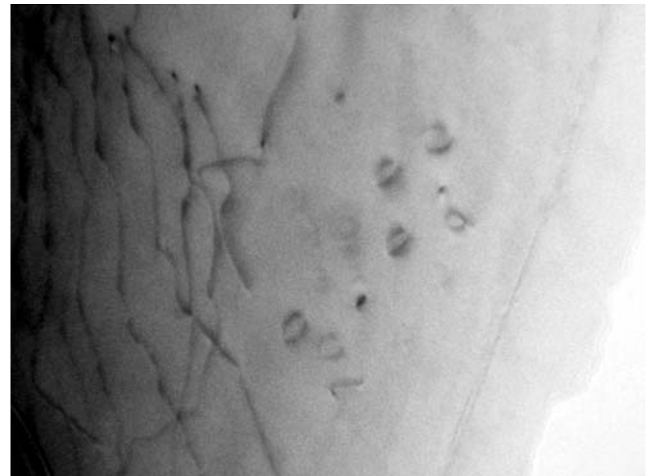

Figure 1: *TEM of fractured tether of aluminum contact metal microtensile specimen. The dark lines on the left are dislocations; note their absence toward the right, near the fracture edge.*

The transmission electron microscope (TEM) micrograph in Figure 1 shows two different deformation mechanisms for a thin aluminum film. Prismatic vacancy loops, seen as circular features about 20 nm in diameter on the right, are formed in the absence of dislocations in the thinner part of the deformation zone near the fracture edge (far right, lower). Dislocations are seen only in the thicker regions, at the left in the image. The size and density of the loops seems to be dependent on the speed of the deformation, with smaller loops 5–10 nm in diameter seen in more slowly deformed material.

Contributors and Collaborators

Y-W. Cheng, J.D. McColskey, R.R. Keller, R. Geiss, J. Wright (Materials Reliability Division, NIST); MOSIS Service (specimen fabrication)

Micrometer-Scale Reliability: Chip-Level Interconnects

Semiconductor manufacturers require increasingly demanding thermal and electrical performance from chip-level interconnects, as feature sizes continue to shrink. Reliability of such small structures then becomes compromised by failure modes unseen by earlier generation interconnect systems. Our studies address thermal and electrical behaviors of interconnects under conditions of extreme stressing. In particular, we concentrate on the roles of localized stress and variations in micro nanostructure in limiting interconnect performance and lifetime. We performed basic studies on aluminum-based structures undergoing AC stressing at high current density (>10 MA/cm^2) as well as measurements of electrical behavior in advanced sub-100 nm copper and silver wires.

Robert R. Keller, Roy H. Geiss, and Yi-Wen Cheng

AC stressing at high-current density and low frequencies is used to simulate the thermomechanical fatigue that can occur during a microelectronic device's operational lifetime, due for example to power cycling, energy saving modes, and to application-specific thermal fluctuations. Cyclic Joule heating takes place, leading to differential thermal expansion between metallic interconnects and surrounding substrates or passivation layers. The resulting damage is due to fatigue mechanisms known to operate in bulk metals, but with the constraints associated with thin films imposed. This year, we performed detailed transmission electron microscope (TEM) studies of the deformation mechanisms, supplementing last year's electron backscatter diffraction studies.

Figure 1 shows a pair of TEM images, bright field (above) and weak beam dark field (below), taken from the same region of a cross section of a severely stressed aluminum interconnect. The image shows a high density of dislocation loops, as indicated by arrows. Analysis of diffraction contrast suggests these to be prismatic loops, where the Burgers vector lies normal to the plane of the loop. Such dislocations can be formed by the coalescence of lattice vacancies into a platelike arrangement. Probable sources of vacancies in thermomechanically deformed metal films include grown-in vacancies or those formed during cross-cutting of screw dislocations.

The existence of prismatic loops suggests a possible means for estimating the local temperature rise during a heating cycle. Such loops are known to disappear after prolonged exposure to high temperatures, as vacancies diffuse out of the film. The observation of these loops after two hours of testing suggests that there was little sustained exposure above approximately 150 °C, which is consistent with our estimates based on electrical resistance measurements. Both a conference proceedings and an archival manuscript are in progress.

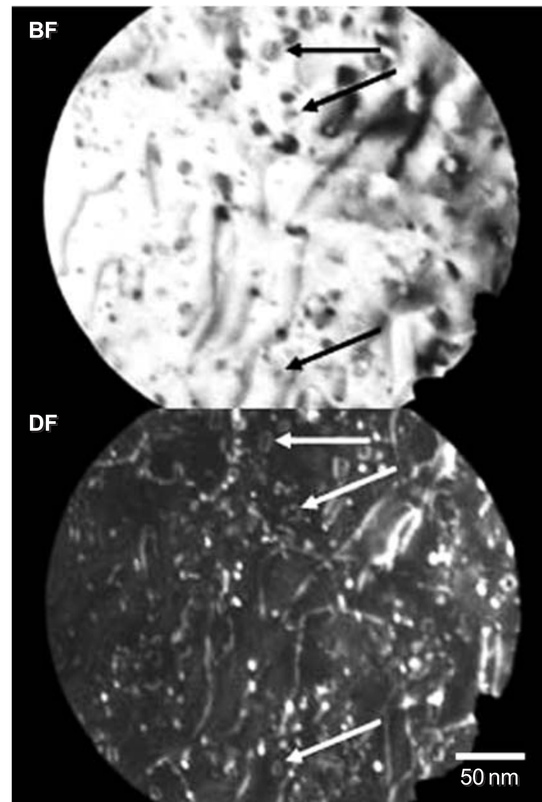

Figure 1: *TEM images showing dislocations induced during high-current density AC stressing in aluminum.*

We also completed, in collaboration with Metallurgy Division, a study of linewidth effects on resistivity in narrow (< 50 nm) silver interconnects fabricated by patterned electrodeposition. We found that resistivity increases could be attributed to electron scattering from interconnect surfaces. More details are provided in the *Metallurgy Division Annual Report* for fiscal year 2004. A manuscript is now in press for *Journal of Applied Physics*.

Contributors and Collaborators

D. Josell (Metallurgy Division, NIST); C. Burkhard (Clarkson University); C. Witt (Cookson Electronics–Enthone)

Micrometer-Scale Reliability: Dynamic Imaging of Magnetic Domain Walls

The purpose is the development of high-sensitivity, low-noise magnetic sensors for use as metrological tools in health care, homeland security and general information technology. In health care, non-invasive sensors are needed for medical evaluation in the areas of magneto-cardiography and magnetic bead tracking of blood flow and stem cells. In homeland security, sensors are needed to detect low levels of pathogens. In IT, sensors are needed for ND failure analysis and magnetic data storage, among others.

Roy H. Geiss

The goal is to develop multi-level magnetic sensors with a sensitivity better than 1 p-tesla/√Hz at 1 Hz noise level that operate at room temperature and can be easily integrated with standard silicon electronics. This involves a many-faceted program that includes materials development, sensor fabrication, sensor characterization, modeling and nanomagnetodynamic imaging. The component being studied here concerns the dynamic observation of magnetic domain walls using Lorentz microscopy in the transmission electron microscope (TEM). Imaging of static magnetic domain walls in the TEM is not new, but our focus is to study the dynamics of domain wall-defect interactions and changes in spin distributions associated with defects or other discontinuities in nanodevices. The ultimate goal is to associate the dynamical interactions with electrical noise measurements in the same sensor.

The effort to image magnetic domain walls has just started. A 200 kV TEM was obtained in 2003. A high-resolution, high-speed CCD camera was installed, and high-resolution, dynamic-magnetic imaging was successfully demonstrated. A sample holder with multiple current feed throughs was designed that allows the application of magnetic fields for *in-situ* testing. Thus far, we have obtained high-resolution images of domain walls at frame rates up to 15 s^{-1}. In particular, we have filmed the formation and movement of Bloch lines and points in cross-tie walls in Ni80Fe20 films 50 nm thick, and have observed the pinning of cross-tie walls at small defects in a noncrystalline CoFeNiSiB alloy film provided by a U.S. magnetic sensor company. Both these dynamic experiments were performed by slowly varying the small local magnetic field in the neighborhood of the specimens in the TEM. Movement of domain walls was possible since the coercivity of both films was very small, on the order of a few oersteds.

The observation of pinning of the domain walls by small defects in the CoFeNiSiB film demonstrated our capability to view interactions in real time. Further, with frame-by-frame analysis of the video, we determined which defects interacted with the domain walls. A few frames from a video sequence containing domain wall pinning are shown in Figure 1. High magnification images of the noncrystalline defects are given in Figure 2.

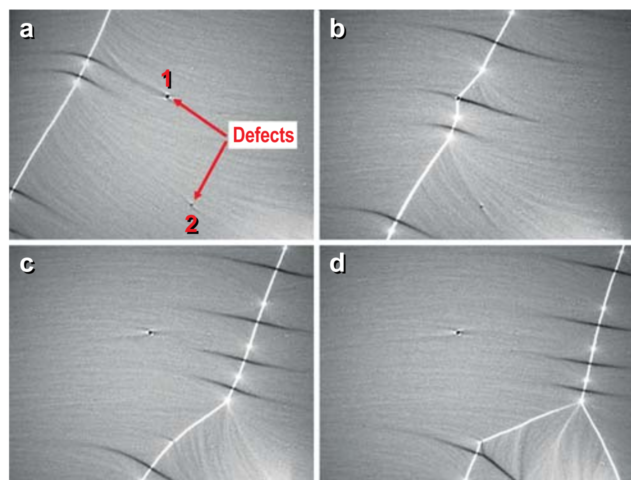

Figure 1: *Images **a** to **d** are from a video sequence showing domain wall pinning. The cross-tie wall seen at the left-hand side in **a** slowly moves to the right under the application of a small magnetic field in **b** through **d**. In **b** the wall is pinned by defect 1. With continued applied field, the wall breaks free from defect 1 and moves to defect 2, where it is again pinned, as suggested in **c** and definitely in **d**. Defects 1 and 2 are 4 µm apart.*

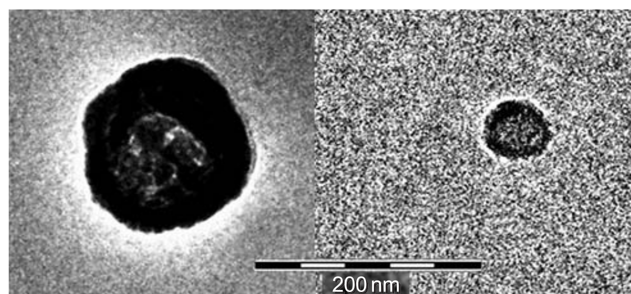

Figure 2: *Images of the individual defects 1 and 2.*

An abstract involving this work has been submitted to the "2004 Magnetism and Magnetic Materials" conference. Studies on smaller structures are the next phase.

Contributors and Collaborators

Steve Russek, Bill Rippard, David Pappas (Magnetic Technology Division, NIST)

Micrometer-Scale Reliability: Bridging Length Scales

We have developed a multiscale model for nanostructures in solids. The model relates the physical processes at the interatomic level to measurable lattice distortions at the nanometer level and macroscopic stresses and strains. The model links the subnano (interatomic), nano (nanostructures), and macro length scales by integrating the powerful techniques of molecular dynamics, lattice-statics Green's functions, and continuum Green's functions.

David T. Read and Vinod K. Tewary

Technical Description

Mathematical modeling is a very important tool for understanding the mechanical behavior of nanomaterials and for research and design of devices based upon nanostructures. A nanostructure needs to be modeled at the following scales: (i) the core region of the nanostructure (subnanometer), where the nonlinear effects may be significant; (ii) the region of the host solid around the nanostructure (nanometer); and (iii) free surfaces and interfaces in the host solid (macro). A nanostructure causes lattice distortion in the host solid that manifests as strain throughout the solid. The strain is essentially a continuum-model parameter, whereas the lattice distortions are discrete variables that must be calculated by use of a discrete lattice theory. Hence, one needs a multiscale model that relates the discrete lattice distortions at the microscopic scale to a measurable macroscopic parameter such as strain.

Conventional models of nanostructures are based upon either the continuum theory, which is not valid close to the defect, or molecular dynamics (MD) which is CPU intensive and usually limited to small crystallites, which may introduce spurious size effects. We need a computationally efficient multiscale model that links the length scales from subnano to macro and that can be used on an ordinary desktop. Such a model will be a valuable tool for research and engineering designs.

Our model is based upon the lattice-statics Green's function (LSGF) **G** that reduces asymptotically to the continuum Green's function (CGF). The displacement field in this model containing N atoms is given by:

$$\mathbf{u}(\mathbf{l}) = (1/N)\, \Sigma_k \mathbf{G}(\mathbf{k})\ \mathbf{F}(\mathbf{k})\ \exp(i\mathbf{k}.\mathbf{l}),$$

where **l** is a lattice site, **k** is a reciprocal space vector, and **F**(**k**) is the Kanzaki force, which is calculated by using MD without making the linear approximation.

For small k, **G**(**k**) reduces to CGF. Thus, for large l, the equation reduces to macroscopic continuum theory while the discrete lattice effects are retained in **F**(**k**). Thus our model is truly multiscale since it seamlessly links the discrete atomistic effects in **F**(**k**) to macroscopic scales through the GF. Even for a million atom model, the calculation of GF takes only a few CPU seconds on a standard 3 GHz desktop.

Accomplishments

Initial conference presentations and a journal paper on this new approach, first reported at the end of FY 2003 and during FY 2004, have been well received.

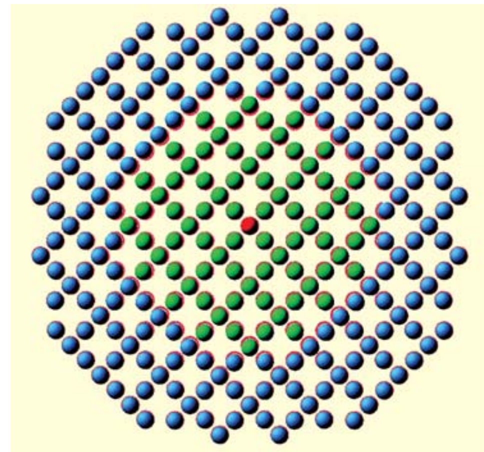

Figure 1: *Section through Ge quantum dot in Si matrix after partial relaxation. The red circles indicate the original positions of the Si lattice sites; the atom in red is the center of the QD.*

This year, we set out to apply the approach to a more timely, but also more challenging, physical system, namely, a germanium "quantum dot" (QD) in a silicon matrix. On the GF side, the challenge was to treat the more complex diamond-cubic lattice structure; on the MD side, the more complex modified embedded atom model potential, needed for silicon and germanium, had to be coded and tested. As of this writing, the first iteration of the Si-Ge quantum dot is in progress. The figure shows the initial distortions of the diamond cubic lattice around a QD with 281 Ge atoms; the method is capable of handling much larger QD, even with a desktop computer.

Contributors and Collaborators

R.R. Keller, Bo Yang (Materials Reliability Division, NIST); E. Pan (Akron University)

Micrometer-Scale Reliability: Molecular Dynamics

It is widely anticipated that applications of nanomaterials will enable major advances in technology in a variety of fields, including sensors, high-strength materials, medicine, and others. Computer simulations seem to offer a path to quantitative understanding of the behavior of nanoscale materials. The form and parameters of the interatomic forces may turn out to be the most concise and useful representation of materials measurement results. Atomistic simulations are widely used in interpreting nanoscale phenomena at the boundary between mechanics and chemistry and to support the plausibility of proposed devices. We are developing the capability to use molecular-dynamics simulations to interpret our own measurements, and to assess the accuracy of proposed interatomic potentials.

David T. Read

Various approaches to simulating atomic interactions have been reported. The **first-principles** approach uses *quantum mechanical* models of nuclei and electrons. Even though this approach typically includes only the valence electrons, it can handle only a few tens of atoms. Recently, in an innovative study, the first principles approach was used to search for new superalloys.

The **molecular-mechanics** approach, widely used for organic molecules such as proteins, requires explicit assumptions about atomic bonding, specifically, a list of which atoms are bonded to which other atoms. The bonds are represented by force laws, and the configuration of complex molecules can be studied. Different force laws may be used for certain types of atoms, depending on the chemical environment. For instance, the carbon–carbon force law in diamond may be different from that in graphite, because of the difference in local chemistry.

Molecular dynamics (MD) treats atoms or molecules as particles that follow *Newton's laws* of mechanics. The particles interact with a prescribed force law, which depends only on the chemical identity of the interacting atoms. The force laws are derived empirically, and the parameters are selected by fitting to measured properties, such as the elastic constants, the vacancy energy, the energy of sublimation, the phonon frequencies, and others. This approach can treat solids, liquids, or gases, and can model melting temperatures and equilibrium crystal structures.

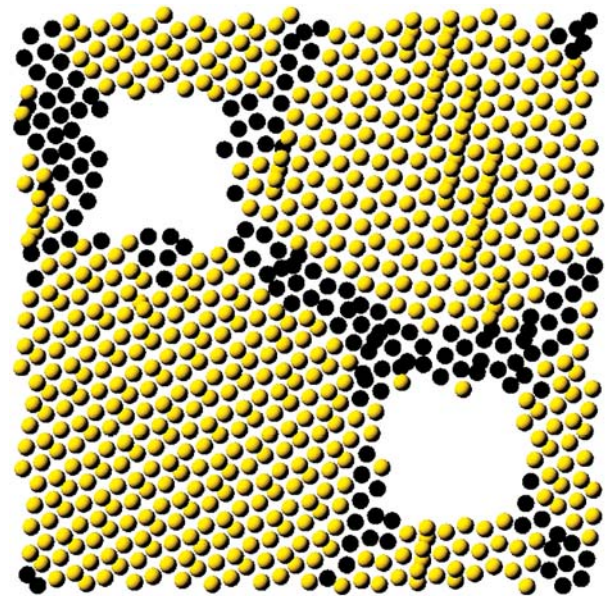

Figure 1: *Cross-section from the center of an array of spheres (AS) model. Atoms shown in color have local fcc symmetry. Atoms shown as black have a lower local symmetry. Because of the periodic boundary conditions, this cell is effectively replicated indefinitely in all 3 dimensions.*

Molecular-dynamics results obtained in the current fiscal year may indicate a mechanism for the recurring reports that the Young's (elastic) modulus values of thin films are lower than those of the corresponding (perfect) bulk material by 10 % or more. Last year's report showed a high-resolution SEM micrograph of electrodeposited copper with a morphology of agglomerated spheres. It's Young's modulus was over 40 % lower than the bulk value. This year, the elastic behavior of a simplified model of such a solid was simulated by molecular dynamics. Caution is in order. The size scale (number of atoms per sphere) and time scale of the simulation were much less than for the actual specimen. The results, averaged over a random set of crystal directions for the spheres, and for two sizes of spheres, produced a Young's modulus 35 % below the bulk value. This was surprising because continuum-mechanics calculations of the modulus decrease produced by defects of like porosity show values proportional to the volume loss. The present MD results are much more dramatic because after the model was brought to equilibrium, it had a density of about 95 % of the bulk value.

Contributors and Collaborators

J. Rifkin (University of Connecticut, author of MD program used)

Micrometer-Scale Reliability: Solder Reliability

The electronics industry is replacing lead–tin eutectic solders with lead-free solders because of the environmental hazards of lead. In doing so, they have created a need for material property data of the new lead-free solder compositions. A test method has been developed to measure the mechanical properties using specimens on the same size scale as the solder structures used in industry.

Timothy P. Quinn

Background

Industry groups have pointed out the need for material property data for the new lead-free compositions of solder; this includes pooling the data that already exist and filling the critical holes in the data, especially at low-strain rates.

Most of the data that are available for all solders come from specimens that are very large (on the order of millimeters) compared to the solder structures themselves (on the order of hundreds of micrometers). As the solder structures (solder balls for flip chip packages, for example) become smaller (~150 µm), their dimensions approach the dimensions of the phases in the solder itself. The assumption of a homogeneous material used to analyze the stresses in the structure is challenged. We have therefore started testing samples that are on the same size scale as current solder structures to study this interaction.

Accomplishments

A test method that used "miniature" specimens was developed to mimic the size of typical soldered joints. The purpose was to examine the effects of the size of the specimens (and hence the typical structures found in industry) and to fill in the gaps in the data for the lead-free solders. Solder was cast in a Ti mold between two copper blocks, and 300 µm specimens were cut from the blocks. The usable gauge length of the specimens was about 300 µm. We can consistently make specimens with a known thermal cycle and maintain well-defined microstructure. Because the samples were sliced off a relatively large "loaf," a large number of samples could be made in a short time.

After determining the geometry of the gage section using an optical microscope, the specimens were imaged in an ultrasonic microscope with a beam diameter of 45 µm at an operating frequency of 100 MHz.

Figure 1: *An ultrasound scan of a solder tensile specimen. The image was made by mapping the amplitude of the reflection off the front interface (white = larger amplitude).*

Measuring the time-of-flight from the front to the rear of the sample allowed us to calculate Young's modulus knowing the density and Poisson's ratio (Figure 1).

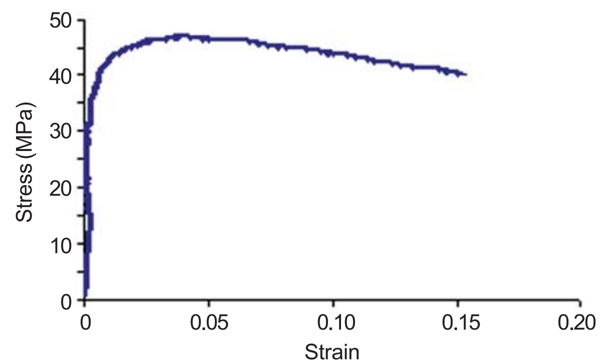

Figure 2: *The measured stress–strain curve for a Sn-3.8Ag-0.7Cu solder.*

The samples were then tested in uniaxial tension using pin-style grips. The specimens were first painted white, and then a dark line was painted on the specimen over the gauge section. A video-microscope recorded images of the gauge section at about 0.75 µm/pixel. The edges of the gauge section were then tracked with an automated algorithm and used to calculate strain. The stress–strain curve was then plotted (for example see Figure 2). Note that because of the small displacements in the elastic region, the camera does not have enough resolution to adequately predict Young's modulus. The ultimate tensile strength, yield strength and percent elongation were all obtained using the camera data. Tests have been conducted using Sn-3.8Ag-0.7Cu, Sn-3.7Ag, Sn-0.7Cu, Sn-5Sb, and Sn-37Pb.

Contributors and Collaborators

Ilan Makover, T.P. Quinn, K.R. Waters (Materials Reliability Division, NIST), Yair Rosenthal (Ben-Gurion University, Israel)

Combinatorial/Phase Diagram Approach for Metallization to Wide-Band-Gap Semiconductors

The development of wide-band-gap semiconductor optoelectronic and electronic devices is hindered by poor electrical contact performance. Reliability issues for contacts include the requirements to be low-resistance, morphologically smooth and thermally stable. This project develops a strategy to improve electrical and morphological characteristics of Ohmic contacts to GaN thin films by optimizing metallization schemes using an integrated phase diagram/combinatorial approach.

Albert V. Davydov and William J. Boettinger

Ti/Al/Ti/Au metallizations are the most commonly used electrical contact to n-type GaN-based device structures. However, the overall composition (*i.e.*, thickness ratios) and the thermal processing of metal layers are not yet optimized. A rationale for designing the optimum metallization scheme also has not been developed. This work demonstrates that the phase diagram approach, along with a combinatorial experimentation method, is a useful tool in the design and optimization of electrical contacts to GaN and other wide-band-gap semiconductors.

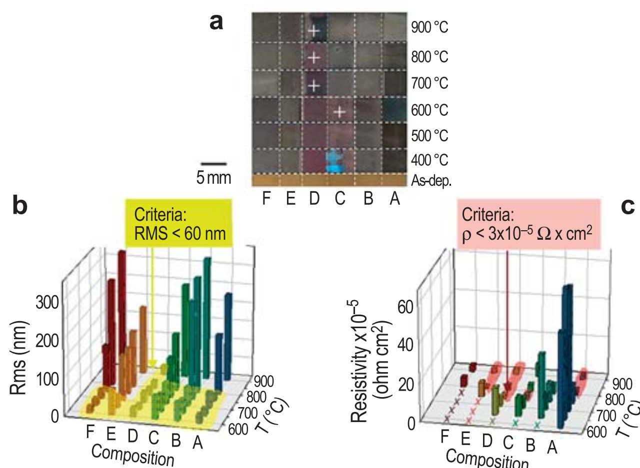

*Figure 1: a) 36-element combinatorial library of annealed Ti/Al/Ti/Au contacts on n-GaN: metal compositions change along the x-axis from A to F, annealing temperature changes from 600 °C to 900 °C along the y-axis; "**X**"s mark the library elements with the lowest resistivity and smoothest morphology; b) map of surface roughness of the combinatorial array: yellow-shaded area represents the contacts with the smoothest (rms < 60 nm) morphology; c) map of electrical resistivity of the combinatorial array: red-shaded area represents the contacts with the lowest ($\rho < 3 \times 10^{-5}\ \Omega \times cm^2$) resistivity.*

A combinatorial library of Ti/Al/Ti/Au metallization was prepared and characterized electrically and microstructurally in order to establish optimum composition and processing parameters for the realization of high-quality Ohmic contacts. An array of metallic elements with varying Ti/Al/Ti/Au thicknesses was deposited by combinatorial ion-beam sputtering (CIBS) on n-GaN/c-sapphire substrate followed by rapid-thermal annealing (RTA) in the 600 °C to 900 °C temperature range. The library design of metal compositions and RTA temperatures was guided using the Al-Au-Ti phase diagram so that various Ti/Al/Ti/Au contact compositions represented different regions on the phase diagram.

Four-probe transmission-line-method and Hall electrical measurements were used to assess contact resistivity and GaN sheet resistance. X-ray diffraction, white-light interferometric microscopy, atomic-force microscopy, field-emission scanning-electron-microscopy, and transmission-electron-microscopy were used to evaluate the microstructure and morphology of contacts and the metal/GaN interfaces. The most Au-rich/Ti-poor metallization (E in Figure 1a), Ti(20 nm)/Al(85 nm)/Ti(15 nm)/Au(150 nm) with an RTA of 800 °C/30 s in argon, produced the lowest ($\rho = 1.3 \times 10^{-5}\ \Omega \times cm^2$) contact resistivity with reasonable (rms < 150 nm) surface morphology. However, the most Al-rich metallization (D in Figure 1a), Ti(20 nm)/Al(170 nm)/Ti(5 nm)/Au(50 nm) with RTA of 750 °C/30 s in argon, produced superior surface morphology (rms = 20 nm) and comparable resistivity of $\rho = 2.2 \times 10^{-5}\ \Omega \times cm^2$. It is suggested that scheme (E) with the Au-rich contact can be used for operating in oxidizing environments, where thick Au top layer will serve as a protective cap layer, while scheme (D) can be suitable for applications where contact surface roughness is critical. According to XRD results, the superior surface morphology of contacts in the D-series correlates with the absence of phase transformations in the 600 °C to 900 °C temperature interval after the initial formation of Al_2Au and Al_3Ti phases in metal films.

The advanced metallizations developed in the project will be validated in industrial high-electron mobility transistors (HEMTs) at Northrop–Grumman Corporation.

Contributors and Collaborators

L.A. Bendersky, D. Josell, U.R. Kattner, A.J. Shapiro (Metallurgy Division, NIST); J.E. Blendell, R.S. Gates, P.K. Schenck, M.D. Vaudin (Ceramics Division, NIST); T. Zheleva (Army Research Laboratory); H.G. Henry (Northrop–Grumman); Q.Z. Xue (Intematix Corp.); A. Motayed (Howard University); I. Takeuchi (Univ. of Maryland)

Lead-Free Surface Finishes: Sn Whisker Growth

As the microelectronics industry moves towards Pb-free assemblies, reliability has become a major concern. Pb-free coatings of nearly pure tin, used as a protective layer to maintain solderability on Cu leadframes and connectors, tend to grow "whiskers" which can cause shorts across component leads. Copper additions to the Sn protective layer have been considered by industry since the Sn-Cu-Ag is likely to be the Pb-free bulk solder of choice for industrial applications. However, measurements made at NIST indicate that the addition of Cu tends to promote whisker growth. Our goal is to better understand how copper and other solutes impact the growth of whiskers on electrodeposited Sn.

Gery R. Stafford, William J. Boettinger, and Kil-Won Moon

Whiskers are generally believed to grow to relieve residual stress in tin and other coatings. However, the origin of this stress has not been definitively determined. The addition of certain solutes, such as Bi and Pb, are known to retard whisker growth in electrodeposited tin coatings, while solutes, such as Zn are known to promote growth. Previous work at NIST has shown that low levels of Pb reduce the residual compressive stress in Sn-Pb electrodeposits, while the addition of Cu increases the residual compressive stress. Current research focuses on the influence of solute type and concentration on residual film stress, stress relaxation, and whisker formation.

Metallographic analysis of Sn-Cu electrodeposits indicates that the Cu is present as the Cu_6Sn_5 intermetallic compound (IMC) which is observed both in the grains and along the grain boundaries. It is unlikely that significant amounts of this complex IMC are formed directly during deposition. Rather, we believe that the as-deposited alloy is a supersaturated solid solution of Cu in Sn that transforms to an equilibrium mixture of Sn and Cu_6Sn_5 either during or soon after deposition.

In solid solution, Cu is presumed to occupy interstitial sites within relatively large square channels that exist in the body-centered tetragonal (bct) Sn structure. This gives rise to the anomalously fast diffusion of Cu in the c-direction of the Sn lattice. In this configuration, it is assumed that the Cu does not alter the lattice volume of the Sn. It is further presumed that as Cu_6Sn_5 precipitates within the deposit, the Cu exits the interstitial sites in the Sn phase and occupies volume more typical of its atomic size; thus, the volume of the entire deposit increases.

We estimate the volumetric strain for Cu_6Sn_5 precipitation from a 1 % Cu solid solution to be about +0.004. The resultant stress generated in the electrodeposit as a result of the IMC precipitation is then on the order of –95 MPa (compressive). This, of course, assumes that Cu_6Sn_5 forms from the solid solution after the deposit has been formed.

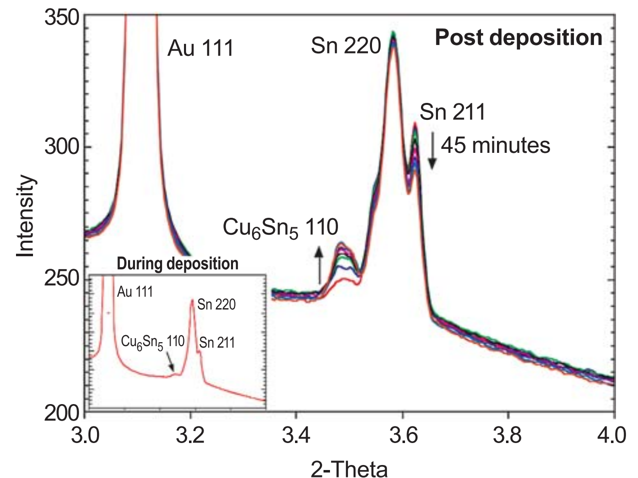

Figure 1: In situ *x-ray diffraction (λ = 0.127 Å) showing growth of the Cu_6Sn_5 110 reflection in the 45 minutes following deposition of bright Sn-Cu alloy from commercial methanesulfonate electrolyte.*

Figure 1 shows a series of x-ray diffraction patterns that were taken at the Advanced Photon Source, using synchrotron radiation, during and after the deposition of a Sn-Cu alloy onto a tungsten substrate. The inset pattern was taken during the 2-minute deposition while the remaining patterns were taken 3 minutes apart after deposition was complete. The data show that although a small amount of Cu_6Sn_5 is present when deposition is stopped (inset), the bulk of the IMC forms in the 45 minutes following deposition. Although the Sn reflections decrease as the IMC forms, the peaks do not change position indicating that the lattice volume of the Sn is constant. This supports the assumption that interstitial Cu does not alter the lattice volume of bct Sn. These results indicate that IMC formation occurs after deposition is complete and is a likely cause of the higher compressive stress observed in Sn-Cu alloy deposits.

Contributors and Collaborators

J.E. Guyer, C.E. Johnson, M.E. Williams (Metallurgy Division, NIST); M.D. Vaudin (Ceramics Division, NIST); D.R. Robinson, D. Wermeille (Advanced Photon Source, ANL)

Lead-Free Solders and Solderability

Solders and solderability are increasingly tenuous links in the assembly of microelectronics as a consequence of ever-shrinking chip and package dimensions and the international movement toward environmentally friendly lead-free solders. In collaboration with the NEMI Pb-Free Assembly Project, we are providing the microelectronics industry with measurement tools, data, and analyses that address national needs in the implementation of lead-free solders.

Ursula Kattner and Carol Handwerker

Since 1999, NIST has served a major role in National Electronics Manufacturing Initiative (NEMI) projects to assist the microelectronics industry implement Pb-free solders. NEMI is an industry-led consortium of approximately 65 electronics manufacturers, suppliers and related organizations brought together to facilitate leadership of the North American electronics manufacturing supply chain. This move toward Pb-free solders is a direct result of the European Union ban, starting in 2006, on Pb-containing solders in electronic products.

NEMI and NIST have worked together to respond to the identified needs by:

1) Identifying and providing the most important lead-free solder data for the microelectronics community (including the definitive database on thermodynamic properties of Pb-free alloys), providing an analysis of the mechanical behavior of Sn-Ag-Cu alloys, and disseminating such data on the NIST website (see "Delivery of Thermodynamics and Kinetic Data" in this volume).

2) Developing and widely disseminating a *Recommended Practice Guide on Test Procedures for Developing Solder Data*.

3) Providing a list of literature references on alloys, processing, reliability, environmental issues, and components for the implementation of lead-free solders.

4) Completing the microstructure-based failure analysis on all thermally cycled assemblies as part of the NEMI project's full-scale reliability trials.

5) Providing chapters on the materials science of Pb-free solder alloys for inclusion in four separate books on Pb-free solder implementation.

Although the NEMI Pb-Free Assembly Project ended in 2003, in 2004 we continued to serve as an information resource to the microelectronics industry on issues related to the effects of alloy composition, reflow temperature and furnace profiles for best melting and solidification behavior of solders when circuit boards are assembled, and to the effects of Pb contamination on alloy melting and assembly reliability. This activity culminated in a *Circuits Assembly* article by Alan Rae, VP of Technology for Cookson Electronics, and Carol Handwerker of NIST on the range of acceptable alloy compositions in the Sn-Ag-Cu system. The following excerpt gives the NEMI position, and effectively the U.S. position, on the acceptable composition ranges for the new international standard Pb-free alloy and allows both the U.S. and the Japanese preferred alloy compositions based on analyses of NIST thermodynamic data:

> Although the composition of some of the alloys being commercialized varies slightly from the NEMI composition, the NEMI alloy is representative of the acceptable range of lead-free solders. Tin–silver–copper formulations with silver content between 3.0 [mass] % and 4.1% and copper between 0.5% and 1.0% are virtually indistinguishable in terms of melting point and process features. The NEMI alloy provides a model system for industry that is well characterized, and several NEMI members currently are using the alloy in production. The focus on a single lead-free alloy has helped to accelerate industry convergence on standard solder formulations, manufacturing processes and, ultimately, the timely and cost-effective conversion to lead-free assembly.

"The NIST group performed a significant service to industry by being the focal point for development of a reliable technology base to support the choice of a new lead-free alloy. They also led the way for further work on issues such as tin whiskers, which emerged from the initial lead-free work. NIST provided not only a strong technical basis but, by verifying reliability and comparing alternatives, enabled industry to choose an alloy based on extensive investigation."

Dr. Robert C. Pfahl, Jr., *Director*
International and Environmental R&D,
Motorola, *(retired)*, and *Vice President*
Operations, NEMI, *(current)*

Contributors and Collaborators

W.J. Boettinger, K.W. Moon, T. Siewert, D. McCowan, L.C. Smith, S.W. Claggett, M.E. Williams (NIST); J.P. Clech (EPSI, Inc.); J. Bath (Solectron); R. Gedney (NEMI); E. Bradley (Motorola); J.E. Sohn (NEMI, formerly Lucent); A. Rau (Cookson Electronics); E. Benedetto (HP); R. Charbonneau (StorageTek)

Electrical Properties of On-Chip Interconnections

Copper wiring in on-chip electrical conductors has reached dimensions so small that electrical resistivity is no longer constant. The higher resistivity induces greater power dissipation, aggravating chip cooling problems. We have quantified the microstructural factors behind this increase for silver wires, where silver has the highest electrical conductivity of any metal.

Daniel Josell and Thomas P. Moffat

As dimensions of transistors in integrated circuits shrink, the dimensions of the metal wires connecting them shrink as well. Dimensions of the wires, and internal grains, are now at approximately 100 nm, similar to the intrinsic mean-free-path lengths of the conduction electrons. Scattering from wire surfaces and grain boundaries is significantly reducing electrical conductivity in such small conductors.

Upcoming dimensional requirements, as specified in the International Technology Roadmap for Semiconductors, require determination of the origin and magnitude of the resistivity increase in order to direct research that might mitigate these size effects.

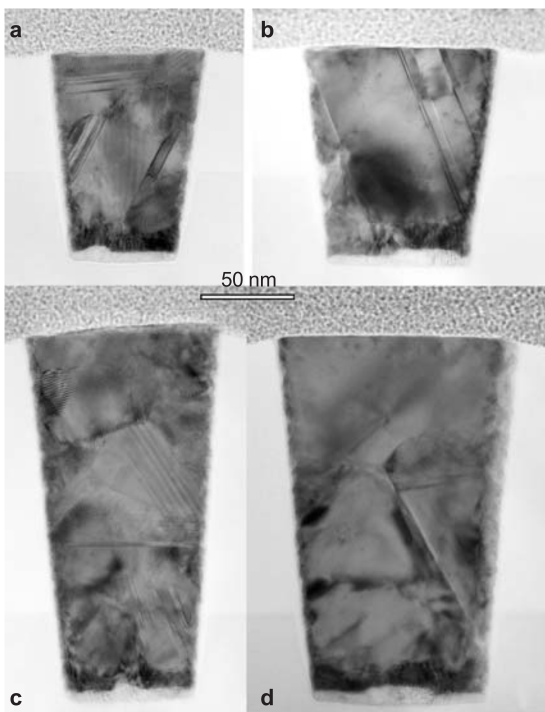

Figure 1: *Transmission electron microscope images of silver wires cross-sectioned after electrical measurement. The higher aspect ratio (height/width) wires contain multiple grains while the lower aspect ratio wires contain only twin boundaries.*

To address these issues, we have measured size-dependent resistivity of silver wires 100 nm to 300 nm tall for widths ranging from approximately 50 nm to 840 nm, produced by electrodeposition on patterned wafers followed by a combined chemical mechanical planarization and oblique ion-polishing process. Silver was selected because of its high electrical conductivity and our recent development of a bottom-up "superfill" process for creating void-free and seam-free wires (Figure 1).

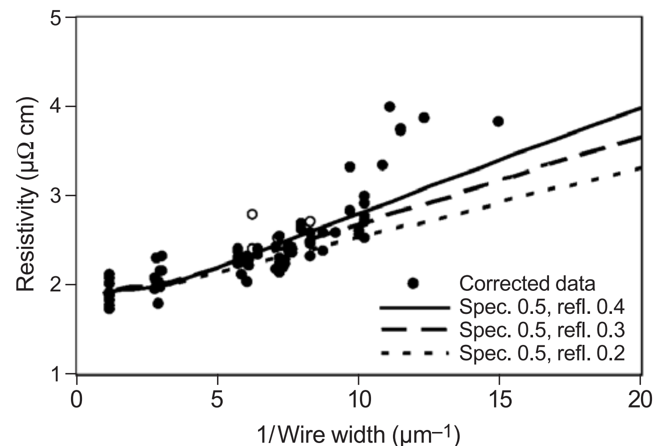

Figure 2: *Electrical properties of 300 nm tall silver wires as a function of the wire width. Curves are the result of calculations including intrinsic, surface and grain boundary scattering of electrons. The sharp increase at ≈ 100 nm is associated with defects.*

To interpret the resistivity data, the Fuchs–Sondheimer formalism (diffuse scattering of electrons on the wire surfaces) was extended to permit a nonzero specular component for surface scattering. The analysis used an existing formalism to account for grain boundary scattering. The resulting equations permit quantitative comparison to experiment (Figure 2).

Significantly, the analysis shows that surface scattering alone is not capable of explaining the observed behavior. Grain boundary scattering is found to contribute a similar, or larger, amount to the overall increase. As a result, the potential payoff of increasing the grain size to decrease grain boundary scattering is recognized to be at least as large as that which might be obtained by smoothing surfaces to increase specularity.

Contributors and Collaborators

G. McFadden (Mathematical and Computational Sciences Division, NIST); R.R. Keller, Y.-W. Cheng (Materials Reliability Division, NIST); C. Witt (Cookson–Enthone); C. Burkhard, Y. Li (Clarkson University)

Nanomagnetodynamics

In order to pursue the rapid development path set out for hard drives and magnetic memory, industry needs the ability to measure and control magnetization on nanometer length scales and nanosecond time scales. This project focuses on the metrology of dynamics and damping in magnetic thin films, especially on the effects of nano-scale dimensions and defects in ferromagnetic resonance measurements.

Robert D. McMichael

We are developing ferromagnetic resonance (FMR) techniques to measure the static and dynamic properties of thin films and patterned arrays of technologically important ferromagnetic metals and their interfaces with normal metals. The primary results include measurements of surface anisotropy, which becomes increasingly important for nanoscale damping, which governs behavior on the sub-nanosecond time scale, and assessment of the magnetic homogeneity of thin films or patterned arrays of magnetic bits. These results are communicated to the magnetic data storage industry through conference presentations, journal articles and site visits.

For nanostructured materials, surface effects and interfacial effects are important. For example, micromagnetic calculations show that switching behavior of magnetic memory cells will be affected by surface anisotropy on the edges of the lithographically patterned elements, an effect that has not been appreciated until recently. Measuring the anisotropy of films of varying thickness with ferromagnetic resonance enables the determination of surface anisotropy values for Permalloy that will be used in the micromagnetic design of MRAM cells.

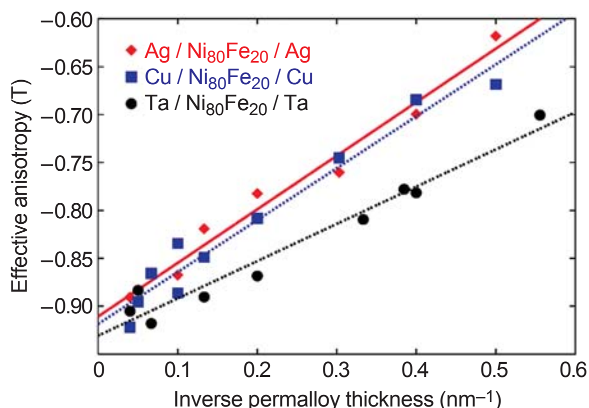

Figure 1: *Surface anisotropy measurements for Permalloy films with different normal metal over/underlayers. The slopes of the fit lines correspond to surface anisotropy.*

A continuing thrust of this project has been the development of models that describe broadening of the FMR linewidth by defects. These models, which are specifically designed for thin films, account for both inhomogeneity and magnetic interactions. Our earlier models were restricted to "local" defects such as anisotropy. One important application of these models is as a method for measurement of anisotropy variations and axis alignment in perpendicular recording media. This year, we have capped off the model development with a model for the non-local effects of film roughness.

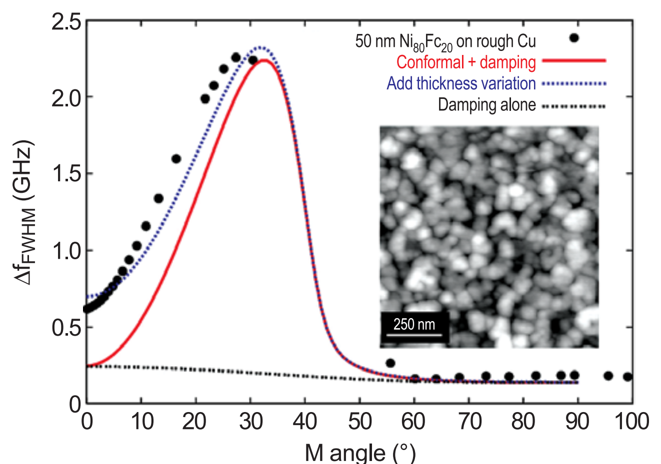

Figure 2: *FMR line broadening measured in a Permalloy film and calculated almost entirely from the microstructure of the underlayer shown in the inset.*

Testing of the roughness-linewidth model involved making variable roughness substrates, characterizing the roughness by atomic force microscopy (AFM), and measuring nearly conformal Permalloy overlayers in FMR. Using only the AFM microstructural data and the known properties of Permalloy, and assuming conformal roughness, the model predictions agreed extremely well with the measurements. Allowing one free parameter describing thickness variations, the agreement with the experiment is nearly perfect. Validation of this model is the first example of linewidth modeling based entirely on the measured microstructure.

Contributors and Collaborators

J.O. Rantschler, B.B. Maranville, J. Mallett, T. Moffat, W.F. Egelhoff, Jr., A.P. Chen (Metallurgy Division, NIST); J.A. Borchers, S.K. Satija (NIST Center for Neutron Research); W. Bailey (Columbia U.); A. Arrott (Virginia State University)

Electrodeposited $Pt_{1-x}(Fe,Co,Ni)_x$ Alloys

Platinum-iron group alloys have at least two important potential applications: as a medium for magnetic recording and as CO tolerant catalysts in fuel cells. Alloy formation by electrodeposition presents a convenient and inexpensive alternative to conventional vacuum methods. A simple thermodynamic model has been used to account for the observed dependence of alloy composition on the deposition potential.

Jonathan J. Mallett, William F. Egelhoff, Jr., and Thomas P. Moffat

Perhaps the most exciting application of iron-group Pt alloys involves their high magnetic coercivity and anisotropy in the $L1_0$ phase. This makes them ideal candidates for future magnetic storage media, which will require high coercivity material to sustain the reductions in bit size needed to increase storage density. Controlled alloy composition and microstructure are essential for achieving the $L1_0$ phase, which requires close to a 50:50 composition.

Iron-group Pt alloys may also find application as poison-resistant hydrogen fuel cell catalysts. A primary concern is the lifetime and efficiency of the catalyst used to oxidize hydrogen gas in the cell. Recent research suggests that replacing the traditional Pt catalyst with a Pt alloy containing up to 15 % of an Fe-group element can dramatically improve the resistance of the catalyst to CO poisoning. An inexpensive, reliable process for producing such alloys is, therefore, likely to be of considerable utility to fuel cell development.

An electrodeposition method has been developed that allows smooth (< 5 nm RMS roughness) alloy films to be deposited to a thickness of between 20 nm and 3000 nm. Deposition takes place from a bath containing 3 mM $PtCl_4$ and 0.1 M of the reactive metal ions (Fe^{2+}, Ni^{2+}, or Co^{2+}). The deposition potentials were chosen such that deposition of the reactive metal in its bulk form would have been energetically impossible. Platinum on the other hand readily deposits at all of the chosen potentials. The incorporation of the reactive metal occurs due to the highly negative enthalpy of mixing of the alloy. This reduces the activity of the reactive element in the alloy and allows its deposition to occur at more positive potentials than would be possible for the pure element. The reactive ions are in much higher concentration than the noble complexed platinum ions, which allows the former to be reduced in a kinetically facile way that enables equilibrium alloy compositions to be achieved. Under these conditions, the alloy composition and morphology was found to remain remarkably invariant to significant perturbations in constituent concentrations. The strong dependence of composition on potential is shown in Figure 1 for three alloys.

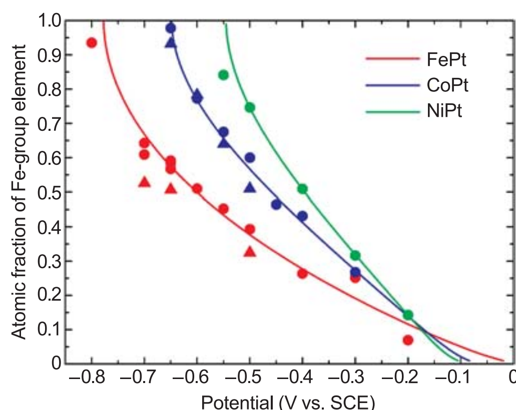

***Figure 1:** The theoretical (curves) and experimental (data points) dependence of composition on potential.*

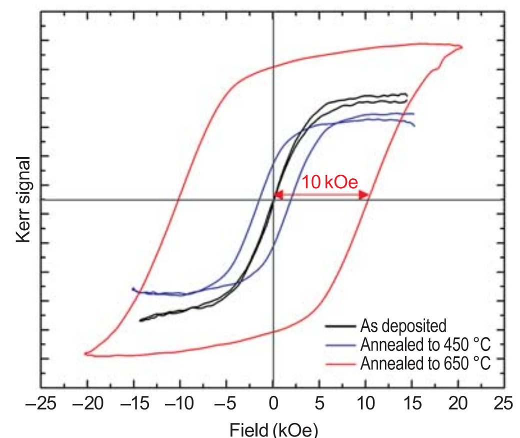

***Figure 2:** The increase in coercivity on annealing.*

Figure 2 shows the effect of annealing an FePt film grown on a Cu(001) substrate. The transformation to the $L1_0$ phase results in a dramatic increase in magnetic coercivity. The 10 kOe coercivity produced by the 650 ºC anneal is suitable for next-generation magnetic media.

Current activities are focused on extending the investigation to ternary alloys and expanding the available deposited structures to include nanoparticles (useful as catalysts) and template-formed nanostructures (for future magnetic recording media).

Contributors and Collaborators

E.B. Svedberg (Seagate Technology)

Novel Magnetic Materials for Sensors and Ultra-High Density Data Storage

Magnetic sensors play a central role in many important technologies ranging from health care to homeland security. A common need among these technologies is greater sensitivity and smaller size. In ultra-high density data storage, one of the most pressing needs is for nano-structured media that store data at ever-increasing densities. Improved methods for the magnetic isolation of grains in ultra-thin films are a key need; we have initiated research programs in both areas.

William F. Egelhoff, Jr.

NIST's Magnetic Engineering Research Facility (MERF) is one of the most versatile facilities in the world for the fabrication and analysis of novel magnetic thin films. Two new areas of research, magnetic sensors and magnetic media, illustrate this versatility. The common link is that both require novel magnetic thin films.

Figure 1: The Magnetic Engineering Research Facility (MERF).

It appears that ultra-sensitive magnetic sensors will require the use of thin films of ultra-soft magnetic alloys. These alloys often have a very complex composition such as $Fe_{73.5}Si_{13.5}B_9Nb_3Cu_1$ and require a very specific annealing process. These materials are well-known in bulk form but have never been produced in thin-film form. The project goal is to carry out the metrology needed to produce these materials as ultra-thin films.

We are presently modifying the MERF to add the capability of ion-beam sputter deposition (IBSD). IBSD, which is based on sputtering a target of the desired composition, is the only reliable method for maintaining the correct composition for complex ultra-thin films. MERF will soon become the only deposition system in the world equipped for ultra-thin film deposition by IBSD, AC and DC magnetron sputtering, and molecular beam epitaxy. Such versatility will allow MERF to continue to play a leading role in magnetic thin-film research.

In the area of novel magnetic media we have been collaborating closely with Seagate. Seagate is the world's leading manufacturer of hard-disk drives, and for the past two years, they have been sending a Ph.D. physicist from their research labs to work with us, first on ballistic magnetoresistance, and now on novel magnetic media.

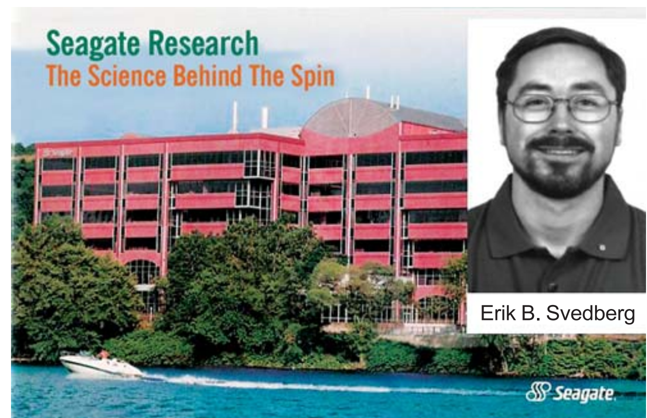

***Figure 2:** Close collaborations with Seagate have contributed to the success of this project.*

Recent work determined a novel method for magnetically decoupling grains in CoPd media. CoPd multilayers are one of the leading candidates for the next generation of magnetic media. We have found that if a Au film is deposited on top of the CoPd and anneal in air, two unexpected phenomena occur as a result of rapid diffusion of atoms along grain boundaries. One is that Co atoms diffuse to the surface, react with oxygen, and remain at the surface. The other is that Au atoms diffuse into the grain boundaries replacing Co. The net effect is that the grain boundaries are demagnetized, and each grain can magnetically switch independently of its neighbors. This method provides the best magnetic isolation of grains yet found.

Contributors and Collaborators

E.B. Svedberg, D. Weller (Seagate); R.D. McMichael, T.P. Moffat, J. Mallett (Metallurgy Division, NIST); D.P. Pappas (Electromagnetics Division, NIST)

Discovery of Spin Density Waves in a Ferromagnet: Fe-Al

Magnetism is endemic to our society. Ferromagnets are the basis for information storage in computers and recording devices; they are found in all motors, transformers, and generators; and they are used in a host of other products like credit cards, cellular telephones, radios, and televisions. However, the magnetic characteristics of the ferromagnet used in each of these applications varies with the product. Consequently, industry needs to know the interconnection between material characteristics and magnetic properties, and how to control them. A critical element in such an understanding is knowledge of the fundamentals of spin interaction, and how to measure it. NIST provides the metrology needed by industry to do this.

Robert D. Shull and Jeffrey W. Lynn (NCNR)

In 1962, a new type of interaction between magnetic spins was predicted — a band structure effect caused by an instability in the conduction electron gas near the Fermi surface. The instability creates a new low-energy state in which the magnetic spin orientations form a standing wave, called a spin density wave (SDW). Similarly, a wave of charge, called a charge density wave (CDW), was also predicted. Charge density waves have since been found experimentally, and the SDW concept has been successfully used to explain the unusual incommensurate antiferromagnetism in Cr. However, evidence for SDWs in a ferromagnet has proven elusive.

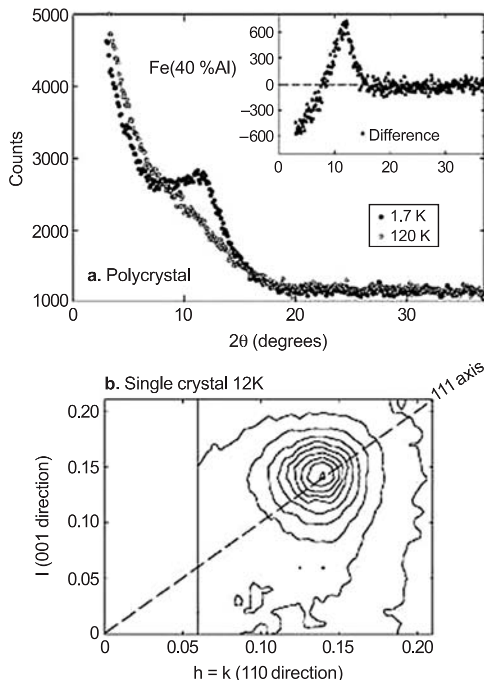

Figure 1: Neutron scattering intensity for a) polycrystalline $Fe_{60}Al_{40}$ at 120 K and 1.7 K with their difference in the inset and b) single crystal $Fe_{60}Al_{40}$ at 12 K shown as contours about the (1/7, 1/7, 1/7) peak.

Using neutron diffraction measurements at NIST, we recently discovered a SDW in a single crystal of $Fe_{60}Al_{40}$, a material with ferromagnetically interacting spins. This was shown (Figure 1) by the presence of scattering intensity at locations where there was no atomic reciprocal lattice vector (*i.e.*, at places where there would normally be no coherent atomic scattering). In fact, the data showed there are several SDWs in the material with wave vectors near (110) directions (shown in Figure 2). No such waves were found along either (100) or (111) directions.

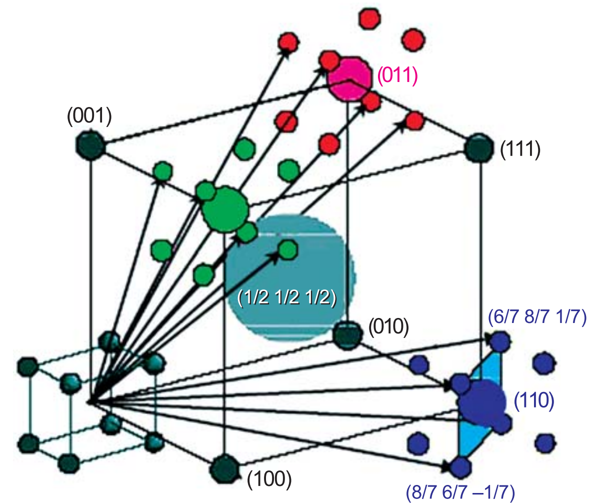

Figure 2:** The reciprocal lattice spots in $Fe_{60}Al_{40}$, showing the SDW wave vectors (black arrows) (*Physical Review Letters ***91, 217201-1 (2004).*

The presence of SDWs shows the exchange interactions between magnetic spins in Fe-Al is a band structure (*i.e.*, non-local) effect and explains the large magnetism in these materials containing a large content of "non-magnetic" atoms. This discovery should be as important to the understanding of magnetism in metals as the SDWs in Cr. In Cr, the SDW wave vector, close to a (100) direction, makes moments of nearest neighbors in the bcc structure almost oppositely aligned.

Contributors and Collaborators

A.S. Arrott (Virginia State University); D.R. Noakes (Virginia State University); M.G. Belk (Virginia State University); S.C. Deevi (Phillip Morris Co.); D. Wu (Dartmouth College)

Characterization of Porous Low-k Dielectric Constant Thin Films

NIST provides the semiconductor industry with unique on-wafer measurements of the physical and structural properties of nanoporous thin films. Several complementary experimental techniques are used to measure the pore and matrix morphology of candidate materials. The data are used by industry to select candidate low-k materials. Measurement methods that may be transferred to industrial laboratories, such as x-ray porosimetry, are developed. New methods are being developed to measure patterned low-k samples and to assess the extent of porous structure modification caused by plasma etch.

Eric K. Lin and Wen-li Wu

The future generation of integrated circuits requires porous low-k interlayer dielectric materials to address issues with power consumption, signal propagation delays, and crosstalk that decrease device performance. The introduction of nanometer scale pores into a solid film lowers its effective dielectric constant. However, increasing porosity adversely affects other important quantities such as physical strength and barrier properties. These effects pose severe challenges to the integration of porous dielectrics into the device structure.

There is a need for nondestructive, on-wafer characterization of nanoporous thin films. Parameters such as the pore size distribution, wall density, porosity, film uniformity, elemental composition, coefficient of thermal expansion, and film density are needed to evaluate candidate low-k materials. NIST continues to develop low-k characterization methods using a combination of complementary measurement methods including small angle neutron and x-ray scattering (SANS, SAXS), high resolution x-ray reflectivity (HRXR), x-ray porosimetry (XRP), SANS porosimetry, and ion scattering. To facilitate the transfer of measurement expertise, a recommended practice guide for XRP was completed and will be available for industrial customers.

In collaboration with industrial and university partners, we have applied existing methods to new low-k materials and developed new methods to address upcoming integration challenges. A materials database developed in collaboration with International SEMATECH is used extensively by SEMATECH and its member companies to help select candidate materials and to optimize integration processing conditions. This year, we also addressed the effects of the ashing/plasma etch process on the low-k material during pattern transfer. Often, surfaces exposed to ashing/plasma densify and lose terminal groups (hydrogen or organic moiety) resulting in increased moisture adsorption and, thus, increased dielectric constant. HRXR measurements enable quantification of the surface densification or pore collapse in ashing-treated and/or plasma-treated blanket films.

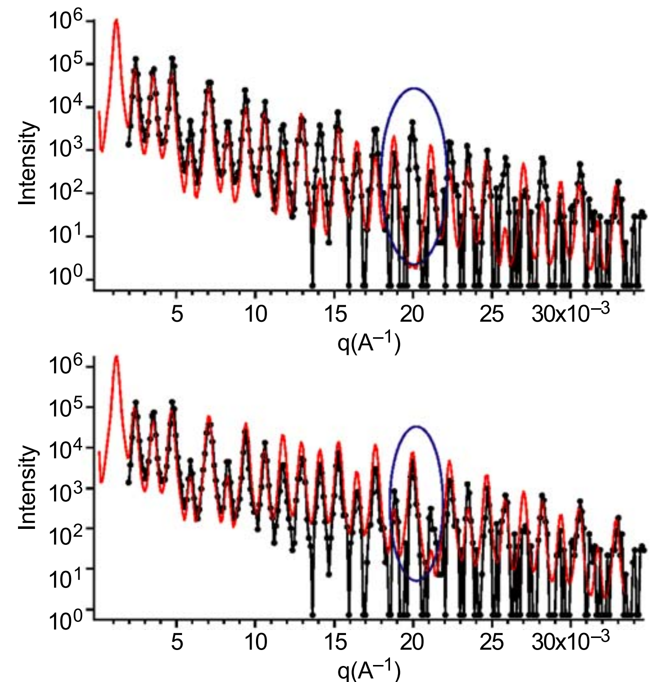

Figure 1: *SAXS data of a test line grating created in a porous low-k film. Experimental data — solid symbol; model fit — red line. The top data was fit with a uniform cross-section whereas the bottom data was fit with a dense skin layer. Regions outlined by blue circle highlight the difference between these two models.*

A new method using SAXS was also developed to investigate the effect of plasma etch on patterned low-k films. Any densification of the sidewall may be observable by x-ray scattering from the cross-section of a patterned nanostructure. Preliminary SAXS work was carried out at Argonne National Laboratory using line gratings of low-k material. The feasibility of this approach is shown in Figure 1 where a surface layer densification is needed to fit the SAXS data.

Contributors and Collaborators

H. Lee, C. Soles, R. Hedden, M. Silverstein, T. Hu, R. Jones, D. Liu, B. Vogt, B. Bauer (Polymers Division, NIST); C. Glinka (NIST Center for Neutron Research); Y. Liu (International SEMATECH); Q. Lin, A. Grill, H. Kim (IBM); M. Ko (LG Chem.); H. Fu (Novellus); J. Quintana, D. Casa (Argonne National Laboratory); K. Char, D. Yoon (Seoul National University); J. Watkins (University of Massachusetts — Amherst)

Polymer Photoresists for Next-Generation Nanolithography

Photolithography, the process used to fabricate integrated circuits, is the key enabler and driver for the microelectronics industry. As lithographic feature sizes decrease to the sub-100 nm length scale, significant challenges arise because both the image resolution and the thickness of the imaging layer approach the macromolecular dimensions characteristic of the polymers used in the photoresist film. Unique high-spatial resolution measurements are developed to reveal limits on materials and processes that challenge the development of photoresists for next-generation sub-100 nm lithography.

Vivek M. Prabhu

Photolithography is the driving technology used by the microelectronics industry to fabricate integrated circuits with ever decreasing sizes. In addition, this fabrication technology is rapidly being adopted in emerging areas such as optoelectronics and biotechnology requiring the rapid creation of nanoscale structures. In this process, a designed pattern is transferred to the silicon substrate by altering the solubility of areas of a polymer-based photoresist thin film through an acid catalyzed deprotection reaction after exposure to radiation through a mask. To fabricate smaller features, next generation photolithography will be processed with shorter wavelengths of light requiring photoresist films less than 100 nm thick and dimensional control to within 2 nm.

To advance this key fabrication technology, we work closely with industrial collaborators to develop and apply high-spatial resolution and chemically specific measurements to understand changes in material properties, interfacial behavior, and process kinetics at nanometer scales that can significantly affect the patterning process.

This year, we have continued to apply and advance unique measurement methods to provide structural measurement of fabricated nanoscale structures and new insight and detail into the complex physico–chemical processes used in advanced chemically amplified photoresists. These methods include x-ray and neutron reflectivity (XR, NR), small angle x-ray and neutron scattering (SAXS, SANS), near-edge x-ray absorption fine structure spectroscopy (NEXAFS), combinatorial methods, solid state nuclear magnetic resonance (NMR), quartz crystal microbalance (QCM), fluorescence correlation spectroscopy (FCS), and atomic force microscopy (AFM).

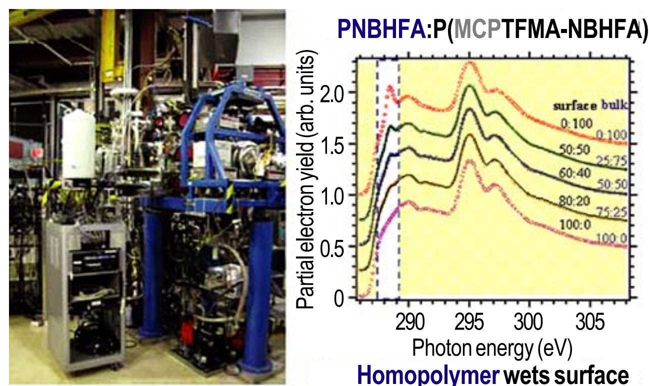

Figure 1: *NEXAFS instrument and spectra illustrating a homopolymer enrichment at the film surface for a model 157 nm photoresist blend. The mismatch in surface versus bulk composition illustrate interfacial limitations for sub 100 nm structures.*

Accomplishments for this past year include: advancement of photoresist–liquid interfaces for immersion lithography and developer distribution in ultrathin films (see highlight); photoresist component segregation (see Figure 1); quantification of the post-exposure bake time on the reaction–diffusion of photoacid 3D deprotection volume; first measurement of immersion and exposure dependence of the surface composition of base additives in 193 nm resist films; identification of key anti-reflective coating (ARC) components responsible for profile control problems and residual layer formation at the ARC-resist interface; quantification of environmental sensitivity by *in-situ* processing using NEXAFS; and quantification of the effects of developer and additives on the final resolution of lithographic features using a model reaction–front bilayer geometry.

International SEMATECH has selected NIST in an effort to apply these fundamental measurements to identify materials sources of the fabrication limits of advanced photoresists.

Contributors and Collaborators

B. Vogt, E. Jablonski, C. Soles, W. Wu, C. Wang, R. Jones, T. Hu, M. Wang, D. VanderHart, C. Chiang, E. Lin (Polymers Division, NIST); D. Fischer, S. Sambasivan (Ceramics Division, NIST); S. Satija (NCNR, NIST); D. Goldfarb, A. Mahorowala, M. Angelopoulos (IBM T.J. Watson Research Center); H. Ito (IBM Almaden Research Center); C. Willson (University of Texas at Austin); R. Puligadda, C. Devadoss (Brewer Science); R. Dammel, F. Houlihan (Clariant Corporation)

Organic Electronics

The field of organic electronics has dramatically emerged in recent years as an increasingly important technology encompassing a wide array of devices and applications including embedded passive devices, flexible displays, and sensors. Device performance, stability, and function critically depend upon charge transport and material interaction at the interfaces of disparate materials. We develop and apply non-destructive measurement methods to characterize the electronic and interfacial structure of organic electronics materials with respect to processing methods, processing variables, and materials characteristics.

Eric K. Lin and Jan Obrzut

Organic electronic devices are projected to revolutionize integrated circuits through new applications that take advantage of low-cost, high-volume manufacturing, nontraditional substrates, and designed functionality. The current state of organic electronics is analogous to the early stages of the silicon electronics industry with the concurrent development of multiple material platforms and processes, and a lack of measurement standardization between laboratories. A critical need exists for new diagnostic probes, tools, and methods to address new technological challenges.

Organic electronics presents fundamentally different measurement challenges from those identified for inorganic devices. The adoption of this technology will be advanced by the development of an integrated suite of metrologies to correlate device performance with the structure, properties, and chemistry of materials and interfaces. We are developing measurement methods to provide the data and insight needed for the rational and directed development of emerging materials and processes.

This year, we have addressed three areas covering a spectrum of active organic electronic materials: dielectric measurements for embedded passive devices, measurements of moisture permeation rates through barrier films for organic light-emitting diode displays, and measurements of the orientation and structure of organic semiconductors for transistor applications.

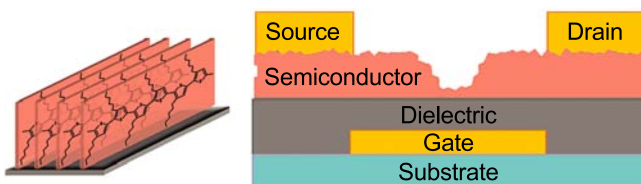

Figure 1: *Schematic diagrams of the local structure of poly 3-hexylthiophene, an organic semiconductor, near an interface (left) and the architecture for an organic transistor (right).*

To meet the metrology needs for embedded passive devices, two new measurement methods were successfully developed and will find widespread use within industry (see Highlight). A NIST-developed *Test Method for Dielectric Permittivity and Loss Tangent of Embedded Passive Materials from 100 MHz to 12 GHz* was accepted and recommended as a standard test method. In addition, a new test was developed and applied for testing passive materials at high electric fields and voltages.

For organic light-emitting diode displays, a key measurement challenge is the quantification of the moisture permeation rates through a barrier coating. Any moisture able to penetrate the coating compromises the performance of the device. There is a need to measure moisture permeation rates as low as 10^{-6} g/m^2 d. In collaboration with Vitex Systems, Inc., neutron and x-ray reflectivity measurements demonstrated the capability of measuring these low permeation rates in addition to providing spatial detail about the transport of water within the barrier material itself.

Finally, near-edge x-ray absorption fine structure (NEXAFS) spectroscopy was applied to several classes of organic electronics materials to investigate the electronic structure, chemistry, and orientation of these molecules near a supporting substrate. NEXAFS provides a powerful and sensitive method to probe the interfacial structure that is critical to the performance of these devices. For example, it was found that several organic semiconductor molecules preferentially align "edge-on" rather than "face-down" on solid substrates.

Contributors and Collaborators

D. DeLongchamp, O. Anopchenko, K. Kano, B. Vogt, H. Lee, E. Jablonski, W. Wu (Polymers Division, NIST); S. Sambasivan, D. Fischer (Ceramics Division, NIST); L. Richter (CSTL); C. Richter, E. Vogel (EEEL); D. McGregor, G.S. Cox, J. Felten (DuPont); D. Fritz (MacDermid); T. Bergstresser (Gould Electronics); K. Fjeldsted (Electro Scientific Industries); R. Crosswell (Motorola); C. Vanderpan (UL); R. Whitehouse (Sanmina-SCI); L. Moro, N. Rutherford (Vitex); V. Subramanian (U.C. Berkeley); Z. Bao (Stanford University); B. Ong (Xerox); A. Afzali (IBM); G. Jabbour (Arizona State University); R. Pilston (Plextronics); Y. Jung, Do Yoon (Seoul National University)

Nanoimprint Lithography

Nanoimprint lithography (NIL) has emerged as a viable next generation lithography (NGL) capable of transferring physical patterns smaller than 5 nm into a polymeric film.[1] *The production of nanoscale structures enabled by NIL raises new metrology challenges, as the ability to pattern now exceeds the ability to measure and/or evaluate material properties. The objective of this project is to develop high-resolution metrologies that facilitate the development of NIL.*

Christopher L. Soles and Ronald L. Jones

NIL has recently emerged as one of the leading NGL candidates for the semiconductor industry. The 2003 update of the *ITRS Semiconductor Roadmap* identifies NIL as a strong candidate lithography for the 45 nm technology node. *Silicon Strategies* included *Molecular Imprints, Inc*. (Austin, TX) and *Nanonex* (Princeton, NJ), two major NIL tool companies, in their "60 Emerging Start-ups" list for 2004. Going beyond CMOS, MIT's *Technology Review* selected NIL as one of the "10 Emerging Technologies That Will Change the World."[2] The cost efficient and high-resolution nanopattering of NIL will also be beneficial in emerging technologies such as optical communications, data storage, bio devices, nano-electromechanical systems (NEMS), micro-electromechanical systems (MEMS), and sensors, by enabling low-cost nanofabrication.

The NIL concept is elegantly simple. A master pattern with sub-100 nm features is fabricated into a hard material (Si, quartz, Ni, etc.) using high-resolution (but slow) patterning, such as e-beam lithography. The patterns are then transferred into a resist by stamping the hard master mold into a softer polymer or monomer film. The pattern is "set" into the resist film with either heat, to facilitate flow into the mold features, or by using a monomeric (liquid-like) film that cross-links in the mold. These imprints can be repeated multiple times using a single master, greatly reducing the cost of ownership.

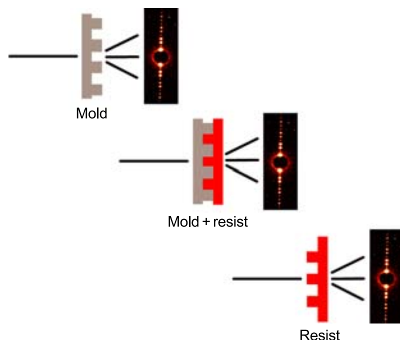

Figure 1: *CD-SAXS quantification of the nanoimprint process.*

One of the greatest challenges facing NIL is to quantify the fidelity of pattern transfer; traditional shape metrologies struggle when feature sizes approach 5 nm. We are developing critical dimension small angle X-ray scattering (CD-SAXS) to quantify 3-D pattern shape, with *sub-nm* resolution. Since CD-SAXS uses high-energy X-rays that penetrate Si and most mold materials, we can quantify pattern shape in the master mold, on the mold in contact with the resist, and in the final pattern (*i.e.*, fidelity of pattern transfer), as depicted in Figure 1.

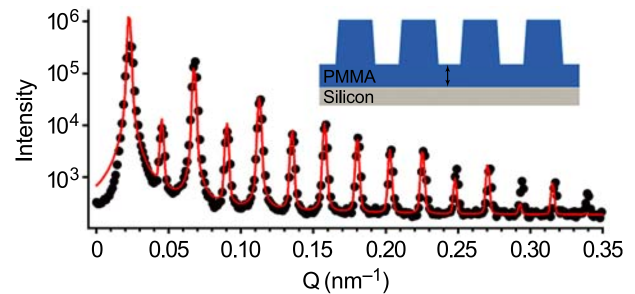

Figure 2: *CD-SAXS data (intensity versus scattering vector) for parallel lines and spaces imprinted into a PMMA film.*

Figure 2 illustrates CD-SAXS data for parallel lines and spaces imprinted into a poly(methyl methacrylate) (PMMA) film. The data are in black, while the red line is a fit to a trapezoidal cross section. By tilting the sample and fitting several data sets, we determine that the pattern pitch is (253 ± 1) nm, the average line width is (146 ± 1) nm, the trapezoid side-wall angle is (4.2 ± 0.5) °, and line height is (180 ± 1) nm.

By providing such accurate structural information, we enable the quantitative evaluation and improvement of imprint processes. Furthermore, we are also developing complementary mechanical and physical property measurements for imprinted polymeric nanostructures. Understanding the unique properties that arise in these nanostructures is crucial to engineering functional and robust polymeric devices at the nanoscale.

References

1. M.D. Austin, *et al.*, *Appl. Phys. Lett.* **84**, 5299 (2004).
2. *Technology Review*, Feb, 42–44 (2003).

Contributors and Collaborators

W. Wu, T. Hu (Polymers Division, NIST); S. Hooker, C. Flannery (Materials Reliability Division, NIST); S. Pang (University of Michigan); C.G. Willson (UT Austin); L. Koecher (Nanonex); D. Resnick, K. Nordquist (Motorola)